Compressive Initial Access and Beamforming Training in Millimeter-Wave Networks

Han Yan, *Student Member, IEEE*, and Danijela Cabric, *Senior Member, IEEE*

***Abstract*—Initial access (IA) is a fundamental physical layer procedure in cellular systems where user equipment (UE) detect nearby base station (BS) as well as acquire synchronization. Due to the necessity of using antenna array in millimeter wave (mmW) IA, the spatial information of channel can also be inferred. The state-of-the-art directional IA (DIA) uses sector sounding beams which fails to provide decent angular resolution and therefore beam training with dedicated radio resources are required. To avoid the extra access latency and overhead, this work proposes to use a quasi-omni pseudorandom sounding beam in IA. In particular, we develop a novel algorithm where the UE can jointly achieve initial access and precise initial beam training without extra radio resources. We study the miss detection rate of the proposed algorithm under synchronization error, and further derive Cramér-Rao lower bound of direction estimation under frequency offset. Using QuaDRiGa simulator with mmMAGIC model, the numerical results show that the proposed approach is advantageous to DIA paired with hierarchy beam training. It offers up to two order of magnitude access latency saving when the same discovery, post training SNR, and overhead performance are targeted and such conclusion holds true in various propagation environment and 3D locations with a mmW pico-cell with up to 140 m radius.**

I. Introduction

Millimeter-wave (mmW) communication is a promising technology for the future cellular network including 5G New Radio (5G-NR) [2]. The mmW network supports ultra-fast data rate due to the abundant bandwidth. As shown in both theory and prototypes, mmW system requires beamforming (BF) with large antenna arrays at both base station (BS) and user equipment (UE) to combat severe propagation loss [3]. Significant change in propagation characteristic and hardware architecture in mmW band require different signal processing techniques [4] and physical layer procedure [5].

Initial access (IA) is one of the fundamental physical layer procedure that is expected to be changed in mmW networks as compared to sub-6GHz band networks. IA allows UE to discover and synchronize with nearby BS before further communication. In mmW system, conventional omni-directionally broadcast IA with single antenna may not be reliable enough. It is the consensus that IA also needs to use transmitter and receiver antenna array [6], [7]. A key challenge is the sounding beam design during IA for reliable discovery. Meanwhile, beam training is an equally important procedure in order to reap the BF gain from large arrays. A key challenge in beam training is to avoid the excessive access latency and signaling overhead during channel probing.

Han Yan and Danijela Cabric are with the Electrical and Computer Engineering Department, University of California, Los Angeles, Los Angeles, CA 90095 (e-mail: yhaddint@ucla.edu; danijela@ee.ucla.edu).

Part of work was presented in IEEE GlobalSIP 2016 [1]

This work was supported by part under NSF grant 1718742.

A. Related works

A number of works investigate sounding beam and processing algorithm design in mmW IA and beam training.

Using directional beam in IA and beam training is investigated in [6]–[15]. Directional IA (DIA) is first studied in [6] and a General Likelihood Ratio Test (GLRT) is proposed to the solve the cell discovery problem with unknown channel and synchronization parameters. The authors also conclude that the directionally beamformed IA signal improves discovery range as compared to omni-directional IA. The DIA is further investigated in [8] where overhead and access latency are analyzed. Work [9] and [10] study DIA in large networks, and access latency is studied using stochastic geometry. Impact of beam-width of sounding beams in DIA is researched in [13]. The comparison between omni-directional and DIA is also discussed in [11]. IA using non-in-band information, e.g., location, sub-6GHz measurement, are discussed in [7], [12]. The above works mostly focus on the overhead and latency for the cell discovery while beam training is not discussed or with coarse resolution [8]. Part of the reasons are that DIA commonly pair with directional beam training [14], [15] where hierarchical sounding beams are used in multiple stages for precise training. However, the user-specific hierarchy sounding beam adaptation introduces latency when the BS is connected with large number of UEs.

The alternative beam training is via the parametric channel estimation [16]–[23]. Exploiting the mmW sparse scattering nature, compressive sensing (CS) can effectively estimate channel parameters using channel observations through sounding beams. Works [16], [17] propose a CS-based narrowband BF training use pseudo-random noise (PN) sounding beams in the downlink, and [18] extends into wideband channel. Other notable works include channel covariance estimation [19]–[21] which requires periodic channel observations, and UE centric uplink training [22], [23]. The above works focus on channel estimation in the dedicated training slots and assume perfect cell discovery and synchronization. The 5G-NR frame structure is rarely considered and thus the feasibility of joint initial access and CS-based beam training are not investigated.

To address the issues of frequency synchronization in narrowband mmW beam training, novel algorithms are proposed in [1], [24]–[26]. Meanwhile, hardware prototypes that use received signal strength (RSS) in CS-based beam training are reported and the signal processing tools include RSS

matching pursuit [27], Hashing table [28], and sparse phase retrieval [29]. However, such phase free measurement is a testbed dependent constraint and does not necessarily apply to all mmW systems. Moreover, the theoretical accuracy limits and practical signal processing algorithm tailored for initial discovery, synchronization, and BF training in mmW frequency selective channel are not yet fully addressed.

B. Contributions

In this work, we propose to use PN sounding beams and novel signal processing algorithm to jointly achieves initial cell discovery, synchronization, and accurate beam training. The contributions are answers to the following questions.

How to use PN sounding beam for IA? We propose an energy detection algorithm for initial discovery and it is tailored for PN sounding beams. We derive the optimal detection threshold, analyze the miss detection probability and the impact of synchronization error, i.e., carrier frequency offset (CFO) and timing offset (TO).

How to reuse received IA signal for beam training? We propose algorithm that re-processes the received IA signal for initial beam training and synchronization once cell detection occurs. We derive the Cramér-Rao lower bound (CRLB) of training performance in line-of-sight (LOS). A CS-based algorithm is proposed that is effective in non-LOS (NLOS) environments and reaches CRLB in LOS.

What are the benefits of compressive IA? We compare the proposed approach with DIA paired by hierarchy beam training. Performance indicators of both approaches are numerically compared, including discovery rate, post beam training SNR, overhead and access latency. The simulation with 5G-NR frame structure and measurement-endorsed 3D mmW channel shows that the proposed approach is advantageous to DIA for UE in various locations of a small cell.

C. Organizations and notations

The rest of the paper is organized as follows. We start with a brief introduction of 5G-NR frame structure, IA and beam training in Section II. In Section III, we present the system model and problem statement. Section IV includes the proposed algorithm for cell discovery and timing acquisition followed by associated performance analysis. In Section V we present the algorithm and analysis for initial beam training under CFO. The access latency, overhead, and complexity analysis is included in Section VI. The numerical results are presented in Section VII. Open research issues are summarized in Section VIII. Finally, Section IX concludes the paper.

Notations: Scalars, vectors, and matrices are denoted by non-bold, bold lower-case, and bold upper-case letters, respectively, e.g. h, $\mathbf{h}$ and $\mathbf{H}$. The (i,j)-th element of $\mathbf{H}$ is denoted by $[\mathbf{H}]_{i,j}$. Conjugate, transpose, Hermitian transpose, and Moore-Penrose pseudoinverse are denoted by $(.)^*$, $(.)^{\mathrm{T}}$, $(.)^{\mathrm{H}}$, and $(.)^\dagger$ respectively. The inner product is $\langle \mathbf{a}, \mathbf{b} \rangle \triangleq \mathbf{a}^{\mathrm{H}}\mathbf{b}$. The l_2-norm of $\mathbf{h}$ is denoted by $||\mathbf{h}||$. $\mathrm{diag}(\mathbf{A})$ aligns diagonal elements of $\mathbf{A}$ into a vector and $\mathrm{diag}(\mathbf{a})$ aligns vector $\mathbf{a}$ into a diagonal matrix. Kronecker and Hadamard product are denoted as $\otimes$ and $\circ$, respectively. $\Re(x)$ and $\Im(x)$ are the real and imaginary parts of a complex element x, respectively.

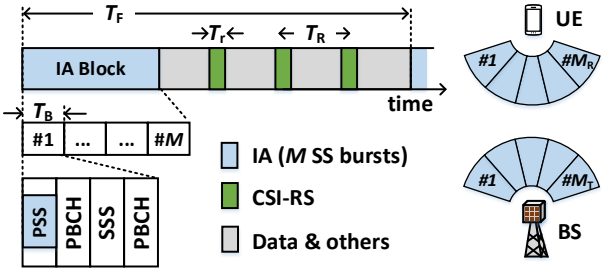

Fig. 1. The 5G-NR mmW frame structure with emphasis in beam management function and the illustration for directional initial access.

II. Preliminary: Initial Access and Beam Training

In this section, we introduce the mmW physical layer frame structure and procedure in 5G-NR cellular network. We briefly review the frame structure, synchronization sequences, and directional IA scheme as well as beam training. Reader are referred to work [7] for a more detailed survey.

Frame Structure: Fig. 1 shows the frame structure of 5G-NR mmW, and we focus on two functional block, synchronization sequence (SS) burst and channel state information reference signal (CSI-RS). 5G-NR uses orthogonal frequency division multiplexing (OFDM), and the subcarrier spacing is either 120 or 240 KHz for mmW band. The SS signal is transmitted by a BS with period T_{F}, typically 20 ms. The SS consists of up to $M = 64$ burst blocks. In each one of the burst block with duration T_{B}, a specific sounding beam pair is used by BS and UE. The CSI-RS block with duration T_{r} is dedicated resource for specific UE(s) for beam training and tracking and CSI-RS has periodicity T_{R}, whose value is implementation dependent.

Synchronization Sequence: Refer to Fig. 1, each SS burst has 4 OFDM symbols, i.e., primary synchronization signal (PSS), physical broadcast channel (PBCH), and secondary synchronization signal (SSS). PSS is used in cell detection and synchronization and they are assigned to the middle $P = 128$ subcarriers of the first OFDM symbols. The PSS is Zadoff-Chu (ZC) sequences in 4G-LTE due to their perfect cyclic-autocorrelation property [30], and becomes Maximum Length Sequences (M-sequences) in 5G-NR [31]. There are 3 and 336 unique sequences of PSS and SSS, respectively, and these 1008 combination defines the cell identifiers (ID) of BS. PBCH carries control information, e.g., channel bandwidth.

Beamformed Initial Access: The BS periodically transmits IA blocks and such signals are processed by UEs which desire to establish the initial access, reconnects after beam misalignment, and search for additional BS for potential handover. The sounding beams in SS bursts intend to facilitate multi-antenna processing in BS and UE when no-priori channel information is available. In the DIA scheme, BS and UE use M_{T} and M_{R} transmitter and receiver beams to cover angular space in both ends and one T/Rx beam is used at a time in the $M = M_{\mathrm{T}}M_{\mathrm{R}}$ SS bursts. Example of such beam sweeping is shown in Fig. 1.

Beam Training: The sounding beams in DIA typically have large beam-width and flat response inside angular sectors [32]. Such design covers the angular space of BS and UE within M bursts, but allows coarse propagation directions estimation [8]. Beam training facilitates higher angular resolution where

TABLE I
NOMENCLATURE

Symbol	Explanations
p, P	Index and total number of subcarriers
m, M	Index and total number of SS bursts
l, L	Index and total number of multipaths
N_{T}, N_{R}	Number of antenna in BS and UE
T_{s}	Sample duration of IA signal
T_{B}, N_{B}	Duration and sample number in each SS burst
T_{F}	Period of SS bursts
T_{R},T_{r}	Period and duration of CSI-RS
N_{c}, N_{cp}	Max. excess delay taps and length of CP
N_{train}, N_{U}	Required CSI-RS and UE number
Δf, ϵ_{F}	CFO in [Hz] and normalized in [rad/samp.]
ϵ_{T}	Initial TO in UE (number of sample)
$\mathbf{H}[d]$	MIMO channel at d-th delay sample
$\mathbf{a}_{\mathrm{T}}(\theta)$, $\mathbf{a}_{\mathrm{R}}(\phi)$	Spatial responses of BS and UE
ϕ_l, θ_l, g_l, τ_l	Gain/AoA/AoD/delay of l-th multipath
α_l, β_l	Real and imaginary parts of g_l
$\mathbf{s}, \tilde{\mathbf{s}}$, $\tilde{s}[n]$	F/T domain PSS vector and sequence
$\mathbf{v}_m, \mathbf{w}_m$	RF precoder/combiner of the m-th burst
$z[n]$, $\mathbf{z}_m$, σ_{n}^2	AWGN sequence, vector, and power
Initial discovery (detection)	
$P_{\mathrm{FA}}^{\star}$	Target FA prob. in initial discovery
$P_{\mathrm{MD,PT}}$, $P_{\mathrm{MD,NT}}$	MD prob. w/ and w/o perfect timing
$\gamma_{\mathrm{PT}}, \eta_{\mathrm{PT}}$	Detection stat. and TH w/ perfect timing
$\gamma_{\mathrm{NT}}, \eta_{\mathrm{NT}}$	Detection stat. and TH w/ unknown timing
Initial beamforming traning (estimation)	
$\boldsymbol{\xi}$	Parameters to estimate in BF training
$\mathbf{y}_m$	Received OFDM symbols at m-th burst
$\mathbf{d}$, $\mathbf{t}$, $\mathbf{r}$	Vectors with candidates delay/AoA/AoD
G_{D}, G_{T}, G_{R}	Parameter grid in delay/AoA/AoD est.
$\mathbf{Q}$, $\mathbf{F}$	ICI matrix and DFT matrix

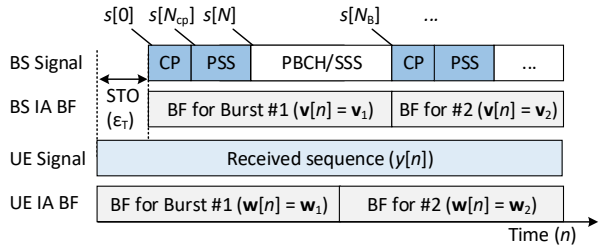

Fig. 2. Illustration of the received signal model as time sequence.

BS and UE steer narrow sounding beams within the sectors of interest. This procedure requires CSI-RS as radio resource.

III. System Model

This section introduces the system model that adopts the above 5G-NR frame structure and problem formulation of the compressive initial access and beam training. All important notations are summarized in Table I.

A. Received signal model before timing acquisition

Consider a single cell system with a BS with N_{T} antennas and it transmits IA signal through mmW sparse multipath channel to UEs. We focus on the BF training procedure of a single UE, and it is straightforward to extend it to multiple UEs since there is no UE-specified adaptive processing. The UE uses analog array architecture, i.e., phased array, with N_{R} antennas, and the single stream of IA signal is transmitted by the BS regardless of its array architecture.

We first consider the received signal model when a UE searches the BS to initialize the connection. In this procedure, UE would assume a periodic SS burst structure and use predefined receiver beamformers to capture signals according to [7]. As illustrated in Fig. 2, when the signal is present, the received sequences with sampling duration T_{s} is denoted as

$$y[n] = \sum_{d=0}^{N_{\mathrm{c}}-1} e^{j(\epsilon_{\mathrm{F}} n + \psi[n])} \mathbf{w}^{\mathrm{H}}[n]\mathbf{H}[d]\mathbf{v}[n-d-\epsilon_{\mathrm{T}}]s[n-d-\epsilon_{\mathrm{T}}] + \mathbf{w}^{\mathrm{H}}[n]\mathbf{z}[n], \quad n \in [0, N_{\mathrm{F}}-1]. \tag{1}$$

In the above equation, ϵ_{T} is the unknown integer sample TO within range[1] $0 \le \epsilon_{\mathrm{T}} \le \epsilon_{\mathrm{T,max}} \le N_{\mathrm{B}}$, where $\epsilon_{\mathrm{T,max}}$ is the largest offset known to the system and N_{B} is the number of samples in one SS burst, i.e., $N_{\mathrm{B}} = T_{\mathrm{B}}/T_{\mathrm{s}}$. The phase measurement error $e^{j(\epsilon_{\mathrm{F}} n + \psi[n])}$ comes from two parts. ϵ_{F} is the normalized initial CFO, i.e., $\epsilon_{\mathrm{F}} = 2\pi T_{\mathrm{s}} \Delta f$ where Δf is absolute CFO in Hz between BS and UE. $\psi[n]$ is the phase noise process in the UE. N_{c} is the maximum excessive multipath delay in discrete time which known to the system in designing cyclic prefix (CP) $N_{\mathrm{cp}} > N_{\mathrm{c}}$ of OFDM symbols, and $s[n]$ is the time domain signals in the SS bursts. We focus on the signal processing of PSS which is mainly used in initial cell discovery and synchronization, and treat other symbols as zero [6], i.e., $s[n] = 0, n \notin \mathcal{S}$, where $\mathcal{S} \triangleq [0, N-1] \cup \cdots \cup [(M-1)N_{\mathrm{B}}, (M-1)N_{\mathrm{B}} + N - 1]$ is the set with sample index corresponding to PSS. Also, we assume a known ZC sequences is used in PSS for mathematical tractability. Specifically, $N = P + N_{\mathrm{cp}}$ is the number of samples of PSS including CP. $\mathbf{z}[n]$ is the additive White Gaussian noise (AWGN) and $\mathbf{z}[n] \sim \mathcal{CN}(0, \sigma_{\mathrm{n}}^2 \mathbf{I}_{N_{\mathrm{R}}})$. Vector time sequences $\mathbf{v}[n]$ and $\mathbf{w}[n]$ are beamformer used by BS and UE at instance n, respectively, and they are from a predefined set of IA beam codebook as part of protocol, i.e., $\mathbf{w}[n] \in \mathcal{W} \triangleq \{\mathbf{w}_1, \cdots, \mathbf{w}_M\}$ and $\mathbf{v}[n] \in \mathcal{V} \triangleq \{\mathbf{v}_1, \cdots, \mathbf{v}_M\}$. BS and UE sequentially uses a beamformer for an interval of N_{B} samples and switch to the next one in $\mathcal{W}$ and $\mathcal{V}$, i.e., $\mathbf{w}[n] = \mathbf{w}_m$, if $\lfloor n/N_{\mathrm{B}} \rfloor = m$ and $\mathbf{v}[n] = \mathbf{v}_m$, if $\lfloor n/N_{\mathrm{B}} \rfloor = m$. Sounding beam switching is assumed not to introduce latency or phase offset in the transmission and reception. In this work, we focus on the system where each element of $\mathbf{v}_m$ and $\mathbf{w}_m$ is randomly and independently chosen from a set[2] $\mathcal{S}_{\mathrm{T}} = \left\{\pm 1/\sqrt{N_{\mathrm{T}}}, \pm j\sqrt{N_{\mathrm{T}}}\right\}$, and $\mathcal{S}_{\mathrm{R}} = \left\{\pm 1\sqrt{N_{\mathrm{R}}}, \pm j\sqrt{N_{\mathrm{R}}}\right\}$. Such sounding beams require only 2 bits phase quantization and have randomized quasi-omnidirectional beam pattern.

The discrete time MIMO channel at delay d ($d < N_{\mathrm{c}}$) is denoted as $\mathbf{H}[d] \in \mathbb{C}^{N_{\mathrm{R}} \times N_{\mathrm{T}}}$. Following the extended Saleh Valenzuela (SV) model in [4], we express $\mathbf{H}[d]$ as

$$\mathbf{H}[d] = \frac{1}{\sqrt{N_{\mathrm{T}} N_{\mathrm{R}}}} \sum_{l=1}^{L} \sum_{r=1}^{R} g_{l,r} p_{\mathrm{c}}(dT_{\mathrm{s}} - \tau_{l,r}) \mathbf{a}_{\mathrm{R}}(\phi_{l,r}) \mathbf{a}_{\mathrm{T}}^{\mathrm{H}}(\theta_{l,r}), \tag{2}$$

[1]We assume coarse timing synchronization is available with 10 μs level accuracy that corresponds to current LTE-A. Practically it is achievable via GPS clock or non-standalone mmW network [7].

[2]The approach and analysis in this work can be extended to other random beamformer design of $\mathcal{S}$, e.g., [4], [22].

where L and R are the number of multipath clusters (typically small, $L \leq 4$ [33]) and sub-paths (rays), respectively. Scalar $g_{l,r}$, $\tau_{l,r}$, $\theta_{l,r}$ and $\phi_{l,r}$ are the complex gain, excessive delay, angle of departure (AoD) and angle of arrival (AoA) of the r-th sub-path within the l-th cluster, respectively. Function $p_{\mathrm{c}}(t)$ is the time domain response filter due to limited temporal resolution T_{s}. With half wavelength antenna spacing, the angular response vectors in the BS and UE are denoted as $\mathbf{a}_{\mathrm{T}}(\theta) \in \mathbb{C}^{N_{\mathrm{T}}}$ and $\mathbf{a}_{\mathrm{R}}(\phi) \in \mathbb{C}^{N_{\mathrm{R}}}$. They are defined by the k-th element as $[\mathbf{a}_{\mathrm{R}}(\phi)]_k = \exp[j\pi(k-1)\sin(\phi)]$ and $[\mathbf{a}_{\mathrm{T}}(\theta)]_k = \exp[j\pi(k-1)\sin(\theta)]$.

Note that the above model aligns with measurement-endorsed mmMAGIC channel model [34] and is used for the system performance evaluation in Section VII. However, for the sake of tractable algorithm design and analysis, the following assumptions and definitions are made.

Assumption 1: BS and UE have ULA with omni-directional element pattern in 2D environment. Intra-cluster AoA, AoD, and delay offsets are zero, i.e., $\phi_{l,r} = \phi_l$, $\theta_{l,r} = \theta_l$, $\tau_{l,r} = \tau_l, \forall r$. Index r is omitted in the rest of paper for clarity. The phase error process is solely from CFO i.e., phase noise process is $\psi[n] = 0, \forall n$ in (1). The complex path gain g_l is deterministic complex value, i.e., $\sum_{l=1}^{L} |g_l|^2 = \sigma_{\mathrm{g}}^2$. The pre-BF signal to noise ratio (SNR) is defined as $\mathrm{SNR} \triangleq \sigma_{\mathrm{g}}^2/\sigma_{\mathrm{n}}^2$.

B. Problem formulations

Two objectives of initial access are considered in this work.

Problem 1 (Initial Discovery and Timing Acquisition): The UE needs to detect the SS burst from BS in mmW band via the received in-band observation (1). This problem is formulated as binary hypothesis testing with unknown channel $\mathbf{H}[d]$ and synchronization errors[3] ϵ_{T} and ϵ_{F}.

$$\begin{aligned} \mathcal{H}_0: \quad & y[n] = \mathbf{w}^{\mathrm{H}}[n]\mathbf{z}[n], \\ \mathcal{H}_1: \quad & y[n] = \sum_{d=0}^{N_{\mathrm{c}}-1} \Big(e^{j\epsilon_{\mathrm{F}} n} \mathbf{w}^{\mathrm{H}}[n]\mathbf{H}[d]\mathbf{v}[n-d-\epsilon_{\mathrm{T}}] \\ & \cdot s[n-d-\epsilon_{\mathrm{T}}] \Big) + \mathbf{w}^{\mathrm{H}}[n]\mathbf{z}[n]. \end{aligned} \tag{3}$$

The TO ϵ_{T} also needs to be estimated in this problem.

Problem 2 (Initial BF Training): The BF training occurs once UE has detected IA signals. In this problem, the UE re-uses the received SS bursts (1) to estimate the unknown parameter vector $\boldsymbol{\xi} \triangleq [\epsilon_{\mathrm{F}}, \theta_1, \phi_1, \tau_1, \alpha_1, \beta_1, \cdots, \theta_L, \phi_L, \tau_L, \alpha_L, \beta_L]^{\mathrm{T}}$, where $\alpha_l = \Re(g_l)$ and $\beta_l = \Im(g_l)$.

Note that cell ID recognition and PBCH decoding are equally important but are left as future works. Moreover, we focus on the AoA/AoD estimation of the most significant path as opposite to the beam training in [18], [22] which intend to estimate entire parametric MIMO channel. This limitation is intrinsic in 5G-NR frame structure where IA sounding use different subcarriers as data communication [7], and thus only angular information probed from IA signal are used.

[3]We focus on regime where CFO is much smaller than OFDM subcarrier spacing, which is up to 240 KHz in 5G mmW.

IV. Initial Discovery and Timing synchronization

In this section, we introduces the proposed initial discovery algorithm using SS burst with PN beams. We also provide theoretical analysis on optimal detection threshold, miss detection rate, and the impact of synchronization errors.

A. Initial discovery and timing synchronization algorithm

Using the correlation filter with known ZC sequence, the UE gets the following signal to design detection statistics.

$$\tilde{y}[n] = \sum_{k=0}^{K-1} y[n+k]s^*[k]. \tag{4}$$

Intuitively, there are M ZC correlation peaks across M SS bursts. The magnitude of the m-th peaks depend on the array gain of the m-th sounding beamformer, CFO, and TO. We propose to use the detector that takes account the sum energy of all energy across M SS burst. Also, different from previous works [6], [9], [10] where threshold is fixed constant, the optimal detection threshold is used from Neyman-Pearson criterion and it meets target false alarm (FA) rate $P_{\mathrm{FA}}^{\star}$.

To understand the impact of timing synchronization error, we first consider a *Genie* scenario where the UE has perfect timing (PT) information of BS. In other words, the system effectively operates at $\epsilon_{\mathrm{T}} = 0$. The proposed mmW PSS detection scheme is an energy detector over all M bursts and therefore a sample time window with N_{c} is used to collect energy from all multipaths. Specifically, the proposed hypothesis testing scheme is expressed as

$$\gamma_{\mathrm{PT}} \triangleq \frac{1}{M} \sum_{m=0}^{M-1} \sum_{k=0}^{N_{\mathrm{c}}-1} |\tilde{y}[k+mN_{\mathrm{b}}]|^2 \underset{\mathcal{H}_0}{\overset{\mathcal{H}_1}{\gtrless}} \eta_{\mathrm{PT}} \tag{5}$$

where the detection threshold η_{PT} is used to reach false alarm rate constraint such that $\Pr(\gamma_{\mathrm{PT}} > \eta_{\mathrm{PT}}|\mathcal{H}_0) = P_{\mathrm{FA}}^{\star}$.

When there is no timing information (NT) available to BS and UE, the proposed mmW PSS detection searches all possible instances within TO window $\epsilon_{\mathrm{T}} \in [0, \epsilon_{\mathrm{T,max}}]$ and uses the highest energy collected for energy detection.

$$\gamma_{\mathrm{NT}} \triangleq \max_{0 \leq n < \epsilon_{\mathrm{T,max}}} \frac{1}{M} \sum_{m=0}^{M-1} \sum_{k=0}^{N_{\mathrm{c}}-1} |\tilde{y}[n+k+mN_{\mathrm{b}}]|^2 \underset{\mathcal{H}_0}{\overset{\mathcal{H}_1}{\gtrless}} \eta_{\mathrm{NT}} \tag{6}$$

The sample indices corresponding to highest energy in (6) is used as TO estimation, namely

$$\hat{\epsilon}_{\mathrm{T}} = \underset{0 \leq n < \epsilon_{\mathrm{T,max}}}{\arg\max} \frac{1}{M} \sum_{m=0}^{M-1} \sum_{k=0}^{N_{\mathrm{c}}-1} |\tilde{y}[n+k+mN_{\mathrm{b}}]|^2. \tag{7}$$

B. Performance of initial discovery and timing acquisition

In this subsection, we provide performance analysis of miss detection rate using the PN IA beam and proposed discovery algorithm, as well as the impact of initial synchronization error ϵ_{F} and ϵ_{T} in discovery and timing acquisition. The exact expression is challenging and tedious, if not impossible and therefore we provide a tight closed-form approximation in the following proposition. To be concise, the subscript of γ and

η that indicates the timing information assumption is denoted as binary variable $\mathrm{z} = \{\mathrm{NT}, \mathrm{PT}\}$.

Proposition 1: The optimal threshold of (6) that reaches target FA rate $\Pr(\gamma_\mathrm{z} \geq \eta_\mathrm{z}^\star | \mathcal{H}_0) = P_\mathrm{FA}^\star$ is approximately[4]

$$\eta_\mathrm{z}^\star = \sigma_\mathrm{n}^2 \left[\frac{N_\mathrm{c}}{P} + \sqrt{\frac{N_\mathrm{c}}{MP^2}} \xi_\mathrm{z} \left(\epsilon_{\mathrm{T,max}}, P_\mathrm{FA}^\star \right) \right], \tag{8}$$

where $\xi_\mathrm{z}(\epsilon_{\mathrm{T,max}}, P_\mathrm{FA}^\star)$ is the threshold adjustment factor defined differently with and without perfect synchronization as

$$\xi_\mathrm{z} = \begin{cases} \mathrm{Q}^{-1}\left(P_\mathrm{FA}^\star\right), & \mathrm{z} = \mathrm{PT} \\ \mathrm{Q}^{-1}\left(\frac{1}{\epsilon_{\mathrm{T,max}}}\right) - \frac{0.78 \ln(-\ln(1-P_\mathrm{FA}^\star))}{\mathrm{Q}^{-1}\left(\frac{1}{\epsilon_{\mathrm{T,max}}}\right)}, & \mathrm{z} = \mathrm{NT} \end{cases}, \tag{9}$$

where $\mathrm{Q}(.)$ and $\mathrm{Q}^{-1}(.)$ are Q-function and inverse Q-function, respectively. The associated miss detection (MD) rate $P_{\mathrm{MD,z}} \triangleq \Pr\left(\gamma_\mathrm{z} < \eta_\mathrm{z}^\star | \mathcal{H}_1\right)$ using the optimal threshold $\eta_\mathrm{z}^\star$ is

$$P_{\mathrm{MD,z}} = \mathrm{Q}\left(\frac{\kappa(\epsilon_\mathrm{T}, \epsilon_\mathrm{F})\mathrm{SNR} - \sqrt{\frac{N_\mathrm{c}}{MP^2}} \xi_\mathrm{z}\left(\epsilon_{\mathrm{T,max}}, P_\mathrm{FA}^\star\right)}{\sqrt{\frac{2\kappa^2(\epsilon_\mathrm{T}, \epsilon_\mathrm{F})\mathrm{SNR}^2}{M} + \frac{N_\mathrm{c}}{P^2 M}}} \right), \tag{10}$$

where the SNR degradation factor $\kappa(\epsilon_\mathrm{T}, \epsilon_\mathrm{F})$ is defined as

$$\kappa(\epsilon_\mathrm{T}, \epsilon_\mathrm{F}) = \frac{2 - \Re\left(e^{jK(\epsilon_\mathrm{T})\epsilon_\mathrm{F}}\right) - \Re\left(e^{j[P-K(\epsilon_\mathrm{T})]\epsilon_\mathrm{F}}\right)}{P^2\left[1 - \Re\left(e^{j\epsilon_\mathrm{F}}\right)\right]}, \tag{11}$$

where $K(\epsilon_\mathrm{T})$ the number of samples during PSS reception that UE switches beamformer due to TO.

$$K(\epsilon_\mathrm{T}) = \begin{cases} N_\mathrm{B} - \epsilon_\mathrm{T}, & \text{if } N_\mathrm{B} - P \leq \epsilon_\mathrm{T} < N_\mathrm{B} \\ 0, & \text{otherwise} \end{cases}. \tag{12}$$

Proof: See Appendix A. ∎

There are two key components in MD expressions (10), namely threshold adjustment factor $\xi_\mathrm{z}(\epsilon_{\mathrm{T,max}}, P_\mathrm{FA}^\star)$ and SNR degradation factor $\kappa(\epsilon_\mathrm{F}, \epsilon_\mathrm{T})$. We have the following observations. Firstly, the CFO affects MD performance by effectively reducing SNR via term $\kappa(\epsilon_\mathrm{F}, \epsilon_\mathrm{T})$. With maximum CFO at UE to be ± 5ppm and typical frame parameters P, M, N_c in Section VII, the SNR degradation is bounded by 4 dB, i.e., $10\log_{10}[\kappa(\epsilon_\mathrm{F}, \epsilon_\mathrm{T})] \geq -4\mathrm{dB}, \forall \epsilon_\mathrm{T}$. Secondly, the TO has impact in both factors. As seen in (11), the SNR in detection degrades when severe TO exists. In fact, it models phenomenon that receiver sounding beam switches during the reception of PSS, i.e., $K(\epsilon_\mathrm{T}) \neq 0$. In addition, the presence of TO forces system to use peak detection scheme (6) where system searches peak location over a sample window with length $\epsilon_{\mathrm{T,max}}$, i.e., the maximum operation in (6). In $\mathcal{H}_0$, the algorithm picks strongest noise realization over $\epsilon_{\mathrm{T,max}}$ samples and thus system needs to use higher threshold than in PT scenario, as seen in (8) and (9). Note that such degradation does not depend on the value of ϵ_T, and the degradation in (10) is not critical with practical maximum TO uncertainty $\epsilon_{\mathrm{T,max}} \leq N_\mathrm{B}$. In summary, synchronization offset does not severely affect discovery performance of the proposed scheme.

[4]Approximation is tight when TO search window size $\epsilon_{\mathrm{T,max}} \geq 100$.

C. Benchmark approach: directional initial discovery

For completeness, we briefly introduce the benchmark approach using directional sounding beam in initial discovery [6]. The system model of DIA is similar to Section III, except the sounding beamformers $\mathcal{W}$ and $\mathcal{V}$ are codebooks that steer directional sector beams, e.g., [14], [35]. Adapting the approach in [6] for the wideband channel and known PSS in SS burst, the cell discovery in DIA uses the following detector

$$\gamma_{\mathrm{DIA}} \triangleq \max_n |\tilde{y}[n]|^2 \underset{\mathcal{H}_0}{\overset{\mathcal{H}_1}{\gtrless}} \eta_{\mathrm{DIA}} \tag{13}$$

where γ_{DIA} and γ_{DIA} are the detection statistic and threshold in DIA. Sequence $\tilde{y}[n]$ is the correlation out in (4) that corresponding to directional sounding beams. We denote $m_{\mathrm{DIA}}^\star$ as the SS burst index associated with the maximum augment in (13) and it is used for hierarchy beam training.

V. Compressive Initial beam training

In this section, we present to initial BF training algorithm where the UE reprocesses the received SS burst signal to extract addition information of the propagation direction. We start with signal rearrangement after successful cell discovery and timing acquisition. Then, we present the compressive sensing formulation followed by the proposed algorithm. Finally, the CRLB and existing approaches, DIA with hierarchy beam refinement, are presented as performance benchmark.

A. Signal rearrangement after timing acquisition

The further processing requires correct detection and CP removal and therefore we made further assumption

Assumption 2: The received IA signal (1) is correctly detected and TO ϵ_T is correctly estimated.

Note that such assumption is valid as presented in Section VII-C. Following assumption, the UE first collects P PSS samples (without CPs) in each of M bursts period from $y[n]$ and rearrange them into vector $\mathbf{y} \in \mathbb{C}^{PM}$, i.e.,

$$\begin{aligned} \mathbf{y} =& [\mathbf{y}_1^\mathrm{T}, \cdots, \mathbf{y}_m^\mathrm{T}, \cdots, \mathbf{y}_M^\mathrm{T}]^\mathrm{T}, \\ \{\mathbf{y}_m\}_p =& y[\hat{\epsilon}_\mathrm{T} + (p-1) + (m-1)N_\mathrm{B}], p \leq P. \end{aligned} \tag{14}$$

For notational convenience of the rest of section, we restate the received signal after CP-removal at the m-th SS burst $\mathbf{y}_m$ according to the system model in Section III,

$$\mathbf{y}_m = \underbrace{\sum_{l=1}^{L} \tilde{g}_{m,l} \mathbf{Q}(\epsilon_\mathrm{F}) \mathbf{F}^\mathrm{H} \left[\mathbf{f}(\tau_l) \circ \mathbf{s}\right]}_{\mathbf{x}_m(\boldsymbol{\xi})} + \mathbf{z}_m, \tag{15}$$

where $\mathbf{x}_m(\boldsymbol{\xi})$ is deterministic vector with the parameter of interest $\boldsymbol{\xi}$ and $\mathbf{z}_m \in \mathbb{C}^P$ is the vectorized random noise. Specifically, in (15) vector $\mathbf{s} \in \mathbb{C}^P$ is the PSS symbols assigned in P subcarriers. Vector $\mathbf{f}(\tau_l) \in \mathbb{C}^P$ is the frequency response of PSS corresponding to the excessive delay τ_l of a multipath, i.e., In other words, the contribution of channel in the p-th subcarrier is

$$[\mathbf{f}(\tau_l)]_p = g_l \exp\left[(-j2\pi(p-1)\tau_l)/(PT_\mathrm{s})\right]. \tag{16}$$

Matrix $\mathbf{F} \in \mathbb{C}^{P\times P}$ is discrete Fourier transform (DFT) matrix. The effective channel gain is defined as $\tilde{g}_{m,l} = e^{j\epsilon_{\mathrm{F}}N_{\mathrm{B}}(m-1)}g_l\mathbf{w}_m^{\mathrm{H}}\mathbf{a}_{\mathrm{R}}(\phi_l)\mathbf{a}_{\mathrm{T}}^{\mathrm{H}}(\theta_l)\mathbf{v}_m$, and it absorbs the phase offset and IA beamformer $\mathbf{v}_m$ and $\mathbf{w}_m$. Diagonal matrix $\mathbf{Q}\in\mathbb{C}^P$ is the frequency offset matrix defined as

$$\mathbf{Q}(\epsilon_{\mathrm{F}}) = \mathrm{diag}\left(\left[1, e^{j\epsilon_{\mathrm{F}}}, \cdots, e^{j(P-1)\epsilon_{\mathrm{F}}}\right]^{\mathrm{T}}\right). \tag{17}$$

Directly estimating $\boldsymbol{\xi}$ from (15) via maximum likelihood (ML) in (15) is conceptually feasible. However, the complexity can be prohibitive due to large number of parameters.

B. Baseline CS formulation

In this subsection, we describe the CS formulation of *Problem 2* and state the intuition of the proposed algorithm.

With straightforward extension of the derivation in [4, Sec. V], the vector $[\tilde{\mathbf{g}}_l]_m = \tilde{g}_{m,l}$ in (15) can be re-formulated as

$$\tilde{\mathbf{g}}_l = \tilde{\mathbf{Q}}(\epsilon_{\mathrm{F}})\tilde{\mathbf{A}}^{\mathrm{H}}\mathrm{vec}(\tilde{\mathbf{H}}_l), \tag{18}$$

where $\tilde{\mathbf{A}}\in\mathbb{C}^{G_{\mathrm{T}}G_{\mathrm{R}}\times M}$ is defined by the Hermitian conjugate of its m-th column as $([\tilde{\mathbf{A}}]_m)^{\mathrm{H}} = (\mathbf{v}_m^{\mathrm{T}}\otimes\mathbf{w}_m^{\mathrm{H}})(\mathbf{A}_{\mathrm{T}}^*\otimes\mathbf{A}_{\mathrm{R}})$. Note that the above equation is different to [4, Sec. V] which requires M^2 sounding beam pairs. The matrix $\tilde{\mathbf{Q}}(\epsilon_{\mathrm{F}})\in\mathbb{C}^{M\times M}$ contains the phase rotation in each SS burst due to CFO.

$$\tilde{\mathbf{Q}}(\epsilon_{\mathrm{F}}) = \mathrm{diag}\left(\left[1, e^{jN_{\mathrm{B}}\epsilon_{\mathrm{F}}}, \cdots, e^{jN_{\mathrm{B}}(M-1)\epsilon_{\mathrm{F}}}\right]^{\mathrm{T}}\right). \tag{19}$$

In fact, matrix $\mathbf{A}_{\mathrm{T}}\in\mathbb{C}^{N_{\mathrm{T}}\times G_{\mathrm{T}}}$ and $\mathbf{A}_{\mathrm{R}}\in\mathbb{C}^{N_{\mathrm{R}}\times G_{\mathrm{R}}}$ are the dictionary of angular response with AoA and AoD from grids with G_{T} and G_{R} uniform steps from $-\pi/2$ to $\pi/2$. In order words, the k-th column in $\mathbf{A}_{\mathrm{T}}$ and $\mathbf{A}_{\mathrm{R}}$ are $[\mathbf{A}_{\mathrm{R}}]_k = \mathbf{a}_{\mathrm{R}}([\mathbf{r}]_k)$ and $[\mathbf{A}_{\mathrm{T}}]_k = \mathbf{a}_{\mathrm{T}}([\mathbf{t}]_k)$, respectively, where $\{\mathbf{r}\}_k$ are the vectors that contain angle candidates.

$$[\mathbf{r}]_k = -\frac{\pi}{2} + (k-1)\Delta\phi, \quad [\mathbf{t}]_k = -\frac{\pi}{2} + (k-1)\Delta\theta. \tag{20}$$

Also note that the steps $\Delta\theta$ and $\Delta\phi$ depend on the target resolution. In this work, G_{T} and G_{R} are used as number of steps and namely $\Delta\theta = 2\pi/G_{\mathrm{T}}$ and $\Delta\phi = 2\pi/G_{\mathrm{R}}$. Matrix $\tilde{\mathbf{H}}_l \in \mathbb{C}^{G_{\mathrm{R}}\times G_{\mathrm{T}}}$ contains the complex path gain of the l-th path, i.e., it has 1 non-zero element whose location depends on the AoA and AoD of the l-th cluster in the angular grids.

When $\tilde{\mathbf{g}}_l$ is directly observable and $\tilde{\mathbf{Q}}(\epsilon_{\mathrm{F}})$ is identity matrix, (18) reduces to the baseline CS-based beam training problem in [4, Sec. V], which can be solved by matching pursuit. The proposed approach estimates $\boldsymbol{\xi}$ from (15) by moving forward with three heuristics presented in the following subsections.

C. Delay estimation

In the first step of the proposed algorithm, $\mathbf{Q}(\epsilon_{\mathrm{F}})$ in (15) is treated as identity matrix. Delay of dominant path, say τ_l, with unknown $\tilde{g}_{m,l}$ is estimated by ML approach. Actually, the proposed algorithm uses sparse impulse support $[\mathbf{d}]_q = q\Delta\tau$ to construct a dictionary, where $\Delta\tau = N_{\mathrm{c}}T_{\mathrm{s}}/G_{\mathrm{D}}$ is the step-size of delay candidates. Based on the knowledge of the model (16) and PSS $\mathbf{s}$, the delay estimation is implemented as

$$\hat{q} = \underset{1\le q\le G_{\mathrm{D}}}{\arg\max}\langle\mathbf{p}_q, \bar{\mathbf{y}}\rangle/\|\mathbf{p}_q\|^2 \text{ and } \hat{\tau}_l = [\mathbf{d}]_{\hat{q}}, \tag{21}$$

where $\bar{\mathbf{y}} = \sum_{m=1}^{M}\mathbf{y}_m/M$ is the received PSS samples averaged over M SS burst. The vector $\mathbf{p}_q$ is the PSS samples when the true delay of dominant path is $[\mathbf{d}]_q$, i.e.,

$$\mathbf{p}_q \triangleq \mathbf{F}^{\mathrm{H}}\left[\mathbf{f}\left([\mathbf{d}]_q\right)\circ\mathbf{s}\right], \tag{22}$$

where $\mathbf{f}([\mathbf{d}]_q)$ is by plugin $[\mathbf{d}]_q$ into (16). The estimated delay tap $\hat{\tau}$ facilitates estimation of effective channel gain $\tilde{\mathbf{g}}_l$,

$$\hat{\mathbf{g}}_l = \left(\mathbf{p}_{\hat{q}}^{\mathrm{H}}\otimes\mathbf{I}_M\right)\mathbf{y}, \tag{23}$$

where $\mathbf{I}_M$ is the $M\times M$ identity matrix.

D. Joint AoA, AoD, and CFO estimation

The second step uses a modified matching pursuit to solve CS problem (18) from $\hat{\mathbf{g}}_l$ and it incorporates the existence of CFO in $\tilde{\mathbf{Q}}$. Specifically, the matching pursuit is proposed where in each of the k matching step, the anticipated effective channel response corresponding to an AoA and AoD pair, i.e., $\tilde{\mathbf{A}}_k$, is used evaluate inner product with $\mathbf{g}$. Note that in this step, delay, AoA, and AoD are treated as known and therefore the CFO can be estimated with closed form. Mathematically it is expressed as

$$\hat{k} = \underset{1\le k\le G_{\mathrm{R}}G_{\mathrm{T}}}{\arg\max}\langle\mathbf{Q}(\hat{\epsilon}_{\mathrm{F},k})\tilde{\mathbf{a}}_k, \hat{\mathbf{g}}_l\rangle/\|\tilde{\mathbf{a}}_k\|^2, \tag{24}$$

where $\tilde{\mathbf{a}}_k \triangleq [\tilde{\mathbf{A}}]_k$ from (18). The matrix $\mathbf{Q}(\hat{\epsilon}_{\mathrm{F},k})$ has structure as (17). The input $\hat{\epsilon}_{\mathrm{F},k}$ is the ML CFO estimator corresponding to this AoA/AoD matching step. Specifically, the design relies on the estimator in [36] and $\bar{\mathbf{y}}_k = \tilde{\mathbf{a}}_k^*\circ\hat{\mathbf{g}}_l$ is treated as a tone with frequency ϵ_{F}.

$$\hat{\epsilon}_{\mathrm{F},k} = \frac{1}{N_{\mathrm{B}}}\angle\left(\frac{1}{M-1}\sum_{m=1}^{M-1}[\bar{\mathbf{y}}_k]_m^*[\bar{\mathbf{y}}_k]_{m+1}\right). \tag{25}$$

Operation $\angle(x) = \tan^{-1}[\Im(x)/\Re(x)]$ evaluate angle of complex samples. To get the AoA, AoD, and CFO estimator, index $\hat{k}$ are used in the candidates grids (20) after the following manipulation $\hat{k}_{\mathrm{R}} = \lfloor(\hat{k}-1)/G_{\mathrm{T}}\rfloor+1$ and $\hat{k}_{\mathrm{T}} = \hat{k}-(\hat{k}_{\mathrm{R}}-1)G_{\mathrm{T}}$,

$$\hat{\phi}_l = [\mathbf{r}]_{\hat{k}_{\mathrm{R}}}, \quad \hat{\theta}_l = [\mathbf{t}]_{\hat{k}_{\mathrm{T}}}, \quad \hat{\epsilon}_{\mathrm{F}} = \hat{\epsilon}_{\mathrm{F},\hat{k}}. \tag{26}$$

E. Gradient refinement

The above steps gives delay, AoA, and AoD estimator are restricted in the grid, i.e., elements of $\mathbf{d}, \mathbf{r}$ and $\mathbf{t}$. Grid refinement is a technique to provide off-grid estimation accuracy and approaches include multi-resolution refinement [37], gradient refinement [38], and the Newtonized gradient refinement [39]. In this work, we propose to use first order descent approach. As initialization of refinement, the estimator from previous steps are packed into $\hat{\boldsymbol{\xi}}^{(k)}$ for $k=1$. In the k-th iteration, the following error vector is evaluated

$$\mathbf{e}^{(k)} = \mathbf{y} - \mathbf{x}\left(\hat{\boldsymbol{\xi}}^{(k)}\right), \tag{27}$$

where $\mathbf{y}$ is the received signal after rearrangement as (14). The second term in the above equation is to plug-in $\hat{\boldsymbol{\xi}}^{(k)}$ into parametric model of $\mathbf{x}(\boldsymbol{\xi})$ in (15). In other words, the error vector $\mathbf{e}^{(k)}$ contains the difference between observed signal

sequence and received signal model using current estimated parameters. The complex gain in iteration k is computed as

$$\hat{g}^{(k+1)} = (\boldsymbol{\nabla}\mathbf{x}_g)^{\dagger}\mathbf{y}, \tag{28}$$

where $\boldsymbol{\nabla}\mathbf{x}_g = (\partial\mathbf{x}(\boldsymbol{\xi})/\partial g)|_{\boldsymbol{\xi}=\hat{\boldsymbol{\xi}}^{(k)}}$ is the partial derivative of $\mathbf{x}(\boldsymbol{\xi})$ over parameter g in (15) and plug-in other parameter with $\hat{\boldsymbol{\xi}}^{(k)}$. The refinement steps for delay, CFO, AoA, and AoD are moving towards the gradient on their estimators in the previous iterations. For concise, in the following equation and paragraph we use x to denote the parameter to be refined, i.e., $x = \{\tau, \epsilon_{\mathrm{F}}, \theta, \phi\}$. The refinement steps are

$$\hat{x}^{(k+1)} = \hat{x}^{(k)} + \mu_x \Re\left[(\boldsymbol{\nabla}\mathbf{x}_x)^{\dagger}\mathbf{e}^{(k)}\right], x = \{\tau, \epsilon_{\mathrm{F}}, \theta, \phi\}, \tag{29}$$

where μ_x is the step-size, vector $\boldsymbol{\nabla}\mathbf{x}_x = (\partial\mathbf{x}(\boldsymbol{\xi})/\partial x)|_{\boldsymbol{\xi}=\hat{\boldsymbol{\xi}}^{(k)}}$ are the the partial derivative of $\mathbf{x}(\boldsymbol{\xi})$ in (15) over parameter of interest. The above approach iteratively runs by packing updated parameter into $\mathbf{x}(\hat{\boldsymbol{\xi}}^{(k+1)})$ for the next iteration until the error $\|\mathbf{e}^{(k)}\|^2$ converges or below threshold ϵ_0.

It is worth noting that the proposed approach can be extended to support multi-path training which have been covered by a variety of works in CS-based approaches [16], [18], [20]–[22], [24]–[26]. However, the main motivation of this work is to showcase and analyze pseudorandom sounding beam in the initial access and initial beam training. Thus only metric direct comparable to its counterpart [6]–[13], namely single path training, is emphasized.

The entire algorithm is summarized in Algorithm I.

Algorithm 1 Compressive Initial Discovery and BF Training

Input: Received signal sequence $y[n]$.
Output: Discovery decision; Channel parameters $\{\hat{\phi}_l, \hat{\theta}_l\}$.
% ——— Initial Discovery ———
PSS correlation (4).
Energy detection (6) and timing acquisition (7).
if PositiveDecision **then**
% —— Initial BF Training (Coarse) ——
  Arrange sequence $y[n]$ into vector $\mathbf{y}$ as (14)
  Estimate excessive delay as (21).
  Estimate effective channel gain $\tilde{\mathbf{g}}_l$ as (23)
  Matching pursuit (24) with CFO estimation (25)
  Get AoA, AoD, and CFO estimators in (26).
% —— Initial BF Training (Fine) ——
  while $\|\mathbf{e}^{(k)}\| > \epsilon_0$ in (27) **do**
    Use refinement steps (28) and (29); $k = k + 1$
  end while
  Use $\phi_l^{(k)}$ and $\theta_l^{(k)}$ as BF training results $\hat{\theta}_l$ and $\hat{\phi}_l$
else
  Wait T_{F} and restart.
end if

F. Performance bound of initial BF training in LOS

In this subsection, we provide performance bound analysis of how accurate can UE joint estimate parameter in $\boldsymbol{\xi}$. In this work we focus on the CRLB when channel has $L = 1$ path which corresponding to pure LOS scenario.

Based on (15), the likelihood function is

$$\Pr(\mathbf{y};\boldsymbol{\xi}) = \frac{1}{2\pi\sigma_{\mathrm{n}}^{2MP}}\exp\left(-\frac{\|\mathbf{y}-\mathbf{x}(\boldsymbol{\xi})\|^2}{\sigma_{\mathrm{n}}^2}\right), \tag{30}$$

where $\mathbf{x}(\boldsymbol{\xi}) = [\mathbf{x}_1^{\mathrm{T}}(\boldsymbol{\xi}), \cdots, \mathbf{x}_M^{\mathrm{T}}(\boldsymbol{\xi})]^{\mathrm{T}}$ as introduced in (15) and the log-likelihood function is $L(\mathbf{y};\boldsymbol{\xi}) \triangleq \ln[\Pr(\mathbf{y};\boldsymbol{\xi})]$. The lower bound of estimation variance is given in the following proposition.

Proposition 2: The CRLB of AoA/AoD estimation in the compressive initial BF training stage in LOS environment is

$$\begin{aligned}\mathrm{var}(\hat{\phi}_1) \geq &\mathrm{CRLB}(\hat{\phi}_1) = [\mathbf{J}^{-1}]_{2,2},\\ \mathrm{var}(\hat{\theta}_1) \geq &\mathrm{CRLB}(\hat{\theta}_1) = [\mathbf{J}^{-1}]_{3,3}\end{aligned} \tag{31}$$

where $\mathbf{J} \triangleq \partial^2 L(\mathbf{y};\boldsymbol{\xi})/\partial\boldsymbol{\xi}^2$ is the Fisher Information Matrix (FIM) whose expressions are listed in (34) of Appendix B

Proof: See Appendix B. ■

G. Benchmark approach: hierarchy directional BF training

The directional beam in SS burst facilitates the system to coarse estimate the propagation directions [40]. Although approaches in the existing literatures are not tailored for wideband channel with synchronization offset. The approach is intrinsically robust. Using to the SS burst index that corresponds to the maximum received power and the knowledge of steering angle in directional IA in DIA. In other words, the BF training results are exactly from the center of the $\hat{m}_{\mathrm{R}}$ and $\hat{m}_{\mathrm{R}}$ of sector beam in BS and UE [40], respectively. Note that $\hat{m}_{\mathrm{R}}$ and $\hat{m}_{\mathrm{R}}$ are the estimated angle sector index, which are converted from the SS burst index $m_{\mathrm{DIA}}^{\star}$ in (13), i.e., $\hat{m}_{\mathrm{R}} = \lfloor (m_{\mathrm{DIA}}^{\star} - 1)/M_{\mathrm{T}} \rfloor + 1$, and $\hat{m}_{\mathrm{T}} = m_{\mathrm{DIA}}^{\star} - (\hat{m}_{\mathrm{R}} - 1)M_{\mathrm{T}}$.

Refer to Fig. 1, the large width of sector beam indicates the poor training resolution in DIA. In order to improve the resolution, hierarchy directional beam with narrower beam width are steered within the sector of interest when radio resource CSI-RS is assigned to a particular UE. Multiple CSI-RS can be sequentially used to improve training resolution.

VI. Access latency, overhead and DSP complexity

In this section, we provide analysis of benefit of using the proposed initial discovery and BF training as compared to DIA in term system access latency and overhead.

Extending [7], we propose to use latency model for both SS burst and CSI-RS as shown in Fig. 3. In both IA scheme, the failure of cell discovery introduce penalty of T_{F} for a new IA block. When cell discovery occurs, the additional latency is required for scheduled CSI-RS according to the required number N_{train}. Thus the access latency is

$$T_{\mathrm{latency}} = \sum_{k=0}^{+\infty} P_{\mathrm{MD}}^{k}(1 - P_{\mathrm{MD}})kT_{\mathrm{F}} + \tilde{T}_{\mathrm{R}}N_{\mathrm{Train}} \tag{32}$$

where the first term takes account latency for cell discovery. In the second term, $\tilde{T}_{\mathrm{R}}$ is the average time for the UE to get the scheduled CSI-RS for beam training and it is expressed as

$$\tilde{T}_{\mathrm{R}} = \frac{1}{N_{\mathrm{U}}}\left[\sum_{k=0}^{K_{\mathrm{F}}}\sum_{q=1}^{K_{\mathrm{R}}}((k-1)T_{\mathrm{F}} + qT_{\mathrm{R}}) + \sum_{q=1}^{K_{\mathrm{res}}}(K_{\mathrm{F}}T_{\mathrm{F}} + qT_{\mathrm{R}})\right]$$

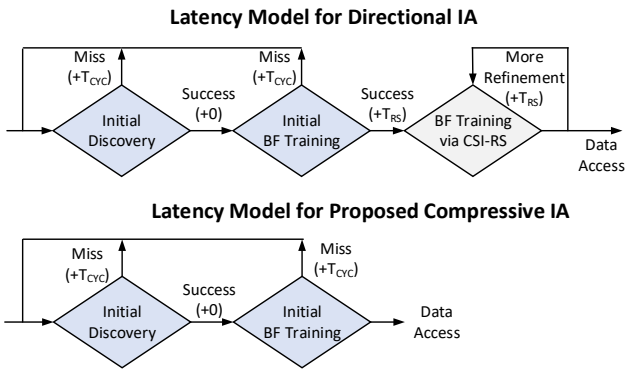

Fig. 3. Initial access latency model for directional IA and the proposed compressive IA. The associated latency in each steps are shown in the bracket.

In the above equation, N_{U} denotes the number of UEs in the network. They share available CSI-RS in a time division manner to combat channel dynamic. Due to the limited number of CSI-RS $K_{\mathrm{R}} = \lfloor (T_{\mathrm{F}} - MT_{\mathrm{B}})/T_{\mathrm{R}} \rfloor$ within one IA period, more than one frame duration is required to meet scheduling to large number of UE N_{U}. Therefore, in (32) the symbol $K_{\mathrm{F}} = \lfloor (N_{\mathrm{U}} - 1)/K_{\mathrm{R}} \rfloor$ is the required number of frame to assign all CSI-RS to UEs and $K_{\mathrm{res}} = N_{\mathrm{U}} - K_{\mathrm{cyc}} K_{\mathrm{R}}$ is the residual delay in the last frame. Note that DIA requires larger N_{train} for more demanding angular resolution while the proposed approach has $N_{\mathrm{train}} = 0$.

The overhead (OH) ratio of IA signals is modeled as follows by counting the time-frequency resource in IA and CSI-RS [7]

$$\mathrm{OH} = \frac{MB_{\mathrm{IA}}T_{\mathrm{B}} + K_{\mathrm{R}}B_{\mathrm{RS}}T_{\mathrm{r}}}{B_{\mathrm{tot}}T_{\mathrm{F}}} \times 100\% \tag{33}$$

where $B_{\mathrm{IA}} = 1/T_{\mathrm{s}}$ is the total bandwidth in IA signals and the channel usage is MT_{s} every SS burst period, T_{F}, and B_{tot} is the total available bandwidth. Particularly, we are interested in the impact of T_{R} on the system performance. Using a reduced period of CSI-RS T_{R} (increased K_{R}) in the frame effectively reduces latency in (32) but increases signaling overhead (33).

The required baseband operations of the proposed algorithm is summarized in Table II, where only the complex multiplications are taken into account as they dominate complexity. As shown in later sections, refinement steps provides CRLB reaching accuracy but is commonly unnecessarily in practical BF training. As a consequence, we do not include the required complexity here. It is worth noting that the above analysis assume the an off-line pre-computation of all required dictionary in matching pursuit, i.e., $\mathbf{p}_q$ in (21), $\tilde{\mathbf{a}_k}$ in (24). On the other hand, the directional IA requires the PSS correlation FIR filter and power evaluations.

TABLE II
DIGITAL BASEBAND OPERATIONS (COMPLEX MULTIPLICATIONS)

Function Block	Equation	Operations
Initial Discovery		
PSS FIR corr.	(4)	PMN_{B}
Detection and time sync.	(5) or (6)	MN_{B}
Initial BF training		
Excess. delay est.	(21) and (23)	$PG_{\mathrm{D}} + PM$
AoA/AoD est.	(24)	$PM + MG_{\mathrm{T}}G_{\mathrm{R}}$
CFO est.	(25)	$2MG_{\mathrm{T}}G_{\mathrm{R}}$

VII. NUMERICAL RESULTS

In this section, we present the numerical results of initial discovery and BF training performance, as well as the associated signaling overhead and access latency.

A. Simulation settings

The simulation follows 3GPP specified frame structure in mmW band. For simplicity, the excessive delay is up to $N_{\mathrm{c}} = 4$ sample duration and a variety of array size options are considered. As for the benchmark directional initial access, we use two approaches to design directional sector beams, i.e., least-square based sector beamforming (LS-Sec) codebook [14] and frequency sampling method based sector beamforming (FSM-Sec) codebook [35]. An example of beam patterns[5] are shown in Fig. 4. In each of the Monte Carlo simulation, independent realization of PN codebook, channel parameter are randomly generated unless otherwise mentioning. Synchronization error in simulation is deterministic as lists for analytical tractability.

The above evaluation uses the simplified SV channel model as described in Section III-A. To evaluate the efficacy of the proposed approach in a realistic 3D mmW environment, in Section VII-C we simulate the system with QuaDRiGa simulator [43] with mmMAGIC model [34], in which we remove *Assumptions 1, 2* in Section III-A and V-A, and use 28 GHz urban-micro (UMi) environment. Uniform planar array (UPA) $N_{\mathrm{T}} = 16 \times 4$, $N_{\mathrm{R}} = 4 \times 4$ are used in BS and UE, respectively, to exploit the higher sparsity in the elevation plane, and the proposed algorithm is extended to 3D accordingly. In the simulation, the transmit signal has 46 dBm power and pathloss and shadow are both used, and AWGN in the receiver is added with $-170 + 10\log_{10}(\mathrm{BW})$ dBm, where $\mathrm{BW} = 1/T_{\mathrm{s}}$ and $\mathrm{BW} = 400$ MHz in IA and data stage, respectively. Moreover, the UE phase noise, $\psi[n]$ in (1), is modeled as Weiner process [44] that corresponds to oscillator with phase noise spectrum -114 dBc/Hz at 1 MHz offset [45], [46]. Frame structure remains as described previously and other detailed simulation setting in QuaDRiGa can be found in the supplementary material [47]. The benchmark approaches are also extended for 3D environment. Specifically, we using FSM-Sec beam designs in both azimuth and elevation plane.

Unless otherwise mentioned, the simulation parameters are summarized in Table. III.

B. Performance in simplified SV channel model

The miss detection rate of the proposed approach in initial discovery is shown in Fig. 5 and it verified the theoretical expressions (10). We have the following findings. Firstly, the lack of perfect timing synchronization introduces around 3 dB sensitivity loss as shown between the blue circled curve and red solid curve. However, it is unavoidable in practice systems. Secondly, less than 3 dB sensitivity loss occur when ± 5 ppm CFO is present, as shown between the blue dashed curve

[5]Sector beam patterns refer to system that has one RF-chain and phase and magnitude control capability in the RF phase shifter [41]. It can also be emitted with more RF-chains when phase-only phase shifters are used [42].

TABLE III
SUMMARY OF SIMULATION SETTINGS

Parameters	Values in Simulations
Frame Structure	
Sub-Carrier Spacing	240 KHz [7]
SS Signal BW	$1/T_s = 57.6$ MHz [7]
Carrier and PSS Length	$P = 128$ [7]
Max Exces. Delay and CP	$N_c = \{4, 32\}$ and $N_{cp} = \{8, 32\}$
SS Burst Duration	$N_B = 1024$ ($T_B = 17.84\mu s$) [7]
SS Burst Num.	$M = 64$ [7]; $M_T = 16$, $M_R = 4$
SS Signal Period	$T_F = 20$ ms [7]
Initial Synchronization Offset	
Freq. Offset at UE	Up to ± 5 ppm [48]
Timing Offset at UE	$\epsilon_T = \{170, 960\}$, ($\Delta\tau = 3, 17\mu s$)
STO Search Window	$\epsilon_{T,max} = 1024$
Algorithm Design	
Target False Alarm	$P^{\star}_{FA} = 0.01$
Dictionary Size	$G_D = 500$, $G_T = 2N_T$, $G_R = 2N_R$

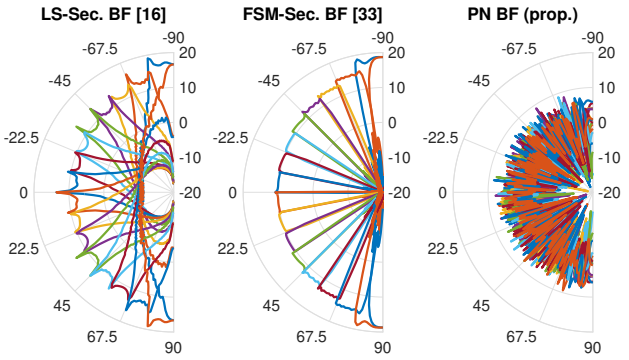

Fig. 4. Beam pattern of two sector beam designs [14], [35] with $M_T = 16$ transmit sectors and one realization of the proposed PN beam. In the polarplot, the r-axis refers to the gain in dB and the angular axis refers to steering angle in degree and all pattern refer to $N_T = 128$ ULA.

and green dashed-and-dotted curve. Finally, the practical TO ($\leq 10\mu s$) is noncritical as shown in red solid and blue dashed curves. But when TO is large enough to causes transmitter and receiver burst beamforming window mismatch, e.g., 17 μs TO, severe sensitivity loss is introduces as shown in grey dotted curves. In summary, simulation verifies the conclusions from Section IV that practical initial synchronization error introduce up to few dB sensitivity loss as compared to ideal scenario. The comparison among proposed and benchmark initial discovery approaches is presented. Although common sense may doubt the efficacy of the proposed approach since there is no significant angular gain in beam pattern, i.e., Fig. 4, the results show there is marginal difference among the proposed approach and benchmark. This is because the proposed scheme collects spread signal energy over all M SS bursts and gives equivalent measurement as directional approach where energy collection is occur when sector beams align with true propagation directions.

The beam training performance of the proposed BF training algorithm in LOS is presented in Fig. 6. The simulation is conducted with assumption that SS burst has been detected and ideal timing acquisition is reached. For tractability, the channel parameter the channel parameter and frequency offsets, $\boldsymbol{\xi}$ and PN beamformer $\{\mathbf{v}_m, \mathbf{w}_m\}$ are deterministic in evaluating CRLB. A same pseudorandom setting is used in both simulation has CRLB evaluation. The performance metrics

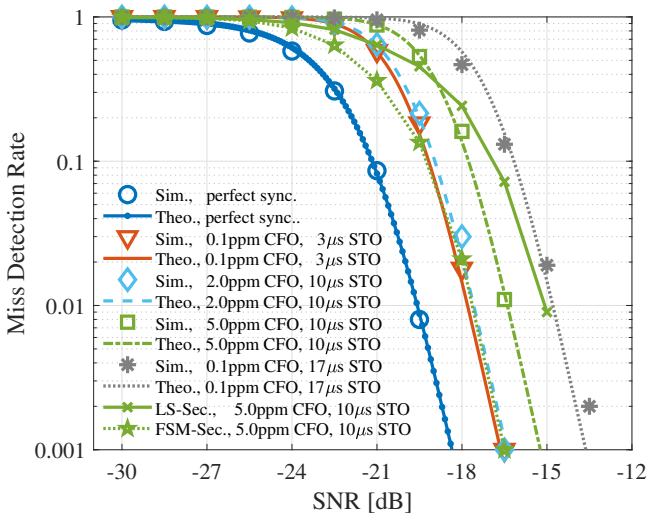

Fig. 5. Simulated (Sim.) and theoretical (Theo.) results of the miss detection rate of the proposed initial discovery with various synchronization errors. The discovery rate of the directional initial access is also included as benchmark and both LS-Sec. and FSM-Sec. are used as sector beams. The BS and UE have $N_T = 128$ and $N_R = 32$ ULA and SV channel has $L = 2$ multipaths.

are the residual mean square error defined by $\text{RMSE}_{\text{AoA}} = \sqrt{\mathbb{E}|\hat{\phi}_1 - \phi_1|^2}$ and $\text{RMSE}_{\text{AoD}} = \sqrt{\mathbb{E}|\hat{\theta}_1 - \theta_1|^2}$. We have the following findings. Firstly, when the refinement steps are used, the proposed algorithm reaches CRLB in high SNR regime. Secondly, the coarse estimation in high SNR has a compromised performance as compared to CRLB. However coarse estimation has accuracy adequate enough for beam steering since RMSE is order of magnitude lower than 3 dB beam-width, i.e., $0.29\pi/N_T$ and $0.29\pi/N_R$ [ref]. Finally, Fig. 5 and 6 reveal that in certain SNR region (-15 to -7.5 dB) reliable detection occurs but beam training performance is poor. Admittedly, this implies to a compromised experience for UEs in the cell edge which worth further investigation[6].

C. Performance in QuaDRiGa channel simulator

Fig. 7 (a) illustrated the network setting in QuaDRiGa. We consider the performance typical UEs distributed in two planes, one is with moderate distance and the other has larger distance that corresponds to the edge of mmW pico cell. We have the following findings in Fig. 7 (b) in terms of post training SNR. Firstly, the proposed approach is comparable with DIA with $N_{\text{train}} = 2$ CSI-RS. In fact, in LOS environment, both approaches are close to beam steering towards true LOS path. Although the SNR seems excessively high in LOS, system designer can simply reduce transmit power to save power. Secondly, DIA with up to $N_{\text{train}} = 2$ CSI-RS has compromised SNR performance. Their drawbacks are intuitive because wide sounding sector beam fails to extract precise angle information. Their SNR degradation versus other curves are more critical in LOS environment since best SNR is captured by perfectly aligning beam with LOS path. Thirdly, although the proposed approach is tailored for sparse channel and phase measurement error due to CFO, it is robust in

[6]It is worth noting that UEs in cell edge are likely to be in NLOS environment, which makes situation more complicated to analyze.

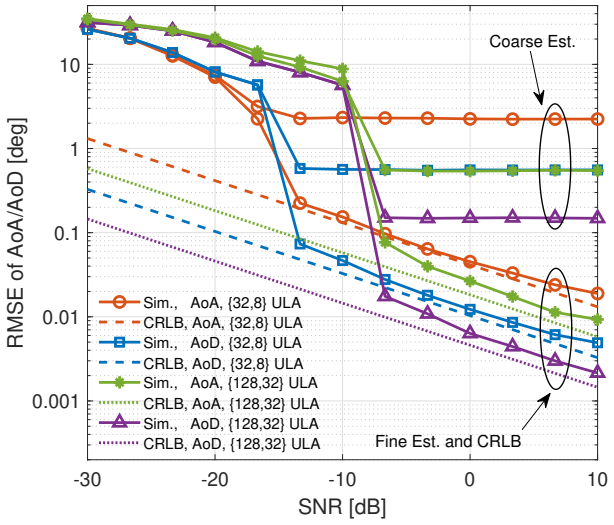

Fig. 6. Simulated results of the proposed algorithm, with and without refinement steps, and theoretical bound of RMSE of AoA/AoD estimation in LOS. Both array geometry setting, $\{N_{\mathrm{T}}, N_{\mathrm{R}}\} = \{32, 8\}$ ULA and $\{N_{\mathrm{T}}, N_{\mathrm{R}}\} = \{128, 32\}$ ULA are evaluated. System has 5ppm CFO.

NLOS scenario when channel sparsity is compromised and practical phase noise occur. Admittedly, it has certain chance to completely fail when NLOS UEs are distributed in the second plane, the counterpart from DIA and CSI-RS cannot do much better jobs. In fact, the proposed approach still have high probability to reach above 0 dB post-training beam steering SNR than state-of-the-art.

The overhead and initial access latency saving is significant when system does not require CSI-RS as shown in Fig. 7 (c). As explained in Section VI, longer access latency when more UEs are in the network since system need to schedule the CSI-RS resource to those UEs. Increasing the density of CSI-RS effectively reduce latency but it is with the cost of increased overhead. The proposed approach relies on advanced signal processing to digitally conduct beam training and avoids requesting CSI-RS in initial access. It results in a initial access latency saving by two order of magnitudes.

D. Baseband processing requirements

Using the parameter in Table III, and a conservative assumption that algorithm re-run every $T_{\mathrm{F}} = 20$ ms, the proposed approach requires 0.27 Giga-operations per second (GOPS) for initial discovery and BF training with high-accuracy. Although exact value of required processing power varies with design, the estimated operation numbers implies that the proposed approach is computational friendly considering the state-of-the-art field-programmable gate array (FPGA) with $\geq$0.1GOPS/mW power efficiency [ref].

VIII. Discussion on Open issues

In this section, we discuss relevant issues in practical implementing compressive IA and beam training.

Required a-priori knowledge: Firstly, this work assumes coarse timing is available. The system is yet to be studied when timing is completely unknown, i.e., no a-priori range information of ϵ_{T} in (1), and possibly SS burst index misalignment occurs. Secondly, the compressive approach requires precise information of the array geometry and the sounding codebook of both BS and UE. It raise challenge in communication protocol design to effectively incorporate different physical array arrangement. The on-line array geometry learning can be an attractive approach for future investigation.

Channel sparsity: The efficacy of compressive approach is affected to the sparsity level in AoA, AoD, and delay. Although sparsity is endorsed by various mmW channel measurement campaign, and urban NLOS is tested in this work, severely unfavorable rich scattering situation may occurs, e,g, there are up to $L = 20$ multipath cluster in the 3GPP specified mmW channel [49]. It is important for system to flexibly handle when channel loses sparsity.

Array architecture: In this work, we focus on the scenario where UE uses a single RF-chain to process a single stream of IA signals. This facilitates other RF-chains, if available in BS or UE, to operate in the band of data communication without pausing in IA. Since [6] shows that the hybrid analog and digital array and fully digital array are advantageous In DIA, it would be interesting to investigate whether this conclusion applies to the compressive IA and beam training approach.

MIMO Multiplexing: The proposed beam training is compatible with MIMO multiplexing in the hybrid array architecture. In fact, designs [23], [50] rely on each RF-chain and corresponding analog beamformer to provide maximum post-BF SNR and uses the digital baseband to handle multi-beam interference. Although its optimality is challenged by recent works [22], it is yet to study whether extra performance is worthwhile with cost of more sophisticated channel training.

Phase coherency: To date, there is no coherent CS-based beam training prototype reported in mmW band. The only notable prototype [51] operates in 8GHz and two phased array are synchronized by cabled reference clock. Except the CFO as emphasized in this work, the phase noise can also severely degrades coherency among channel observations. Their detrimental impact become more severe with increased carrier frequency , e.g., 73, 90, 140GHz and above [52]. Proper phase noise compensation as well as non-coherent CS-based beam training [27]–[29] are naturally immune to phase error is worth investigating.

IX. Conclusions

In this work, quasi-omni pseudorandom sounding beam is proposed for the mmW initial access, synchronization, and beam training. We design associated signal processing algorithm tailored for 5G-NR frame structure and the proposed sounding beam. We provide theoretical analysis of cell discovery rate and beam training performance and evaluated with simulation using the mmW hardware and urban channel model endorsed by measurements. The results showcases that the proposed approach is comparable with the state-of-the-art directional cell search in cell discovery performance, but significantly more accurate in the initial beam training. This advantage holds true across different propagation condition

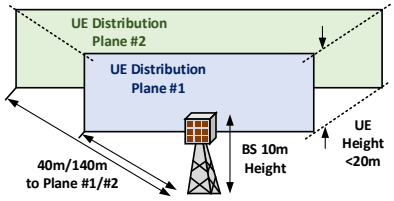

(a) Network illustration where a UE is randomly distributed in the horizontal plane with height of UE within 20 meters.

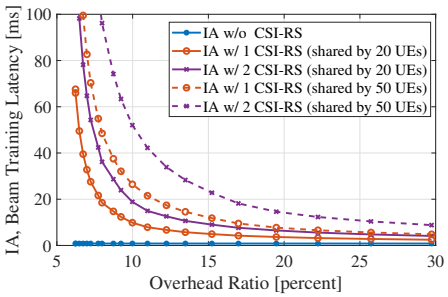

(c) Access latency versus overhead according to model (32) and (33) with different number of UEs that share the scheduled CSI-RS. P_{MD} is 0.04.

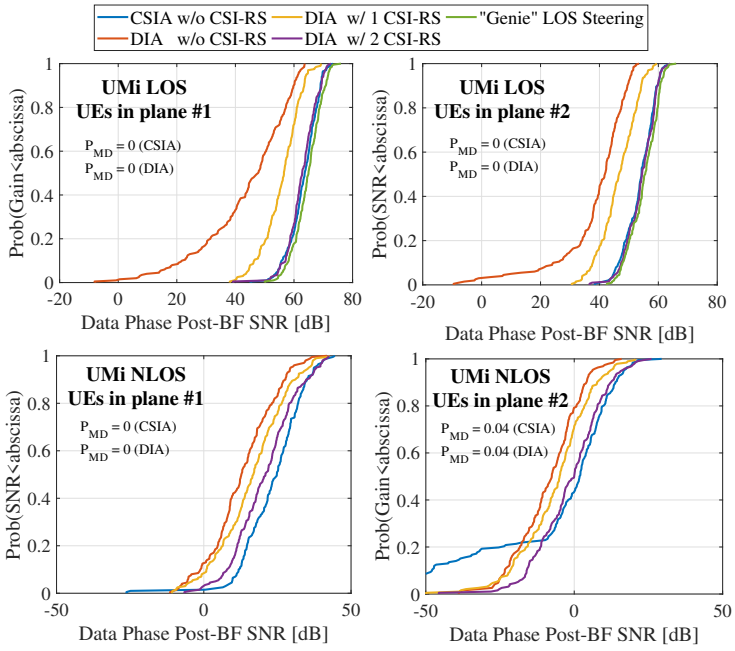

(b) The CDF of post-training beam steering SNR in the data phase. For the DIA, different number of CSI-RS N_{train} are considered. The SNR distribution corresponding to beam steering towards true LOS path (when existing) is also included as benchmark. The miss detection rates are included in each plots.

Fig. 7. Initial access and beam training of proposed and benchmark approaches performance in a realistic 3D outdoor UMi network using QuaDRiGa [43] with mmMAGIC channel model [34]. The trade off between post-training SNR in the data phase, required overhead, and access latency are also studied.

(LOS/NLOS) and UE-BS distance. Due to the saving of additional radio resource (CSI-RS) for beam refinement, the proposed approach reduces up to two order of magnitude access latency versus the directional initial access when the same signaling overhead and post-training beam steering SNR are targeted.

The MATLAB simulation scripts used in this work are accessible in [47].

APPENDIX

A. Initial discovery performance

The noise after autocorrelation $\tilde{z}[n] = \sum_{n=0}^{P-1}(\mathbf{w}^{\text{H}}[n+p]\mathbf{z}[n+p])s^*[p]$ is zero mean complex white Gaussian process with variance σ_{n}^2/P. Therefore $|\tilde{z}[n]|^2$ is Chi-Square random variable with degree-of-freedom 2, mean σ_{n}^2/P, and variance σ_{n}^4/P^2. The detection statistic under $\mathcal{H}_0$ is denoted as $\gamma_{\text{PT},0}$. It is the square-sum of $N_{\text{c}}M$ realizations of $\tilde{z}[n]$ before divided by M and central limit theory (CLT) applies. The mean and standard deviation of $\gamma_{\text{PT},0}$ are $\mu_{\text{PT},0} = N_{\text{c}}\sigma_{\text{n}}^2/P$ and $\sigma_{\text{PT},0} = \sqrt{N_{\text{c}}\sigma_{\text{n}}^4/(P^2M)}$, respectively. As a result, the optimal detection threshold that reaches target false alarm rate $P_{\text{FA}}^\star$ is as (8). Similarly, the detection statistic under $\mathcal{H}_0$ is denoted as $\gamma_{\text{NT},0}$. It is the maximum operation with degree of freedom $\epsilon_{\text{T,max}}$ of $\gamma_{\text{PT},0}$. With large $\epsilon_{\text{T,max}}$, $\gamma_{\text{NT},0}$ follows extreme value distribution, *Gumbel Distribution*, where the mean and standard deviation are $\mu_{\text{NT},0} = \mu_{\text{PT},0} + \sigma_{\text{PT},0}\text{Q}^{-1}(1/\epsilon_{\text{T,max}})$ and and $\sigma_{\text{NT},0} = \sigma_{\text{PT},0}/\text{Q}^{-1}(1/\epsilon_{\text{T,max}})$, respectively. Using its inverse cumulative distribution function, the optimal detection threshold is $\eta_{\text{NT}}^\star = \mu_{\text{NT},0} - (\sqrt{6}\pi)\sigma_{\text{NT},0}\ln(-\ln(1-P_{\text{FA}}^\star))$. It gives (8) using expressions of $\mu_{\text{NT},0}$, $\sigma_{\text{NT},0}$ and $\sqrt{6}/\pi \approx 0.78$.

With perfect synchronization, the detection statistic under $\mathcal{H}_1$ is denoted as $\gamma_{\text{PT},1}$ and it is the sum of signal energy and noise energy $\gamma_{\text{PT},0}$. Therefore $\gamma_{\text{PT},1} = (\sum_{m=1}^{M}\sum_{l=0}^{L}|\tilde{g}_{m,l}\sum_{n=1}^{P}|s[n]|^2|^2)/(MN_{\text{T}}N_{\text{R}}) + \gamma_{\text{PT},0} = \sum_{m=1}^{M}\zeta_m/M + \gamma_{\text{PT},0}$ where $\zeta_m = \sum_{l=0}^{L}|g_l\mathbf{w}_m^{\text{H}}\mathbf{a}_{\text{R}}(\phi_l)\mathbf{a}_{\text{T}}^{\text{H}}(\theta_l)\mathbf{v}_m|^2/(N_{\text{T}}N_{\text{R}})$. Using the fact that ζ_m are mutually independent due to independent $\mathbf{v}_m$ and $\mathbf{w}_m$, the mean of ζ_m is $\mathbb{E}(\zeta_m) = \sum_{l=1}^{L}|g_l|^2\mathbb{E}\left|\mathbf{w}_m^{\text{H}}\mathbf{a}_{\text{R}}(\phi_l)\right|^2/N_{\text{T}}\mathbb{E}\left|\mathbf{a}_{\text{T}}^{\text{H}}(\theta_l)\mathbf{v}_m\right|^2/N_{\text{R}} = \sigma_{\text{g}}^2$ The variance of ζ_m is $\text{var}(\zeta_m) = \sum_{l=1}^{L}|g_l|^4\mathbb{E}\left|\mathbf{w}_m^{\text{H}}\mathbf{a}_{\text{R}}(\phi_l)\right|^4/N_{\text{T}}^2\mathbb{E}\left|\mathbf{a}_{\text{T}}^{\text{H}}(\theta_l)\mathbf{v}_m\right|^4/N_{\text{R}}^2 - \sigma_{\text{g}}^4 = \sigma_{\text{g}}^4\left(2-\frac{1}{N_{\text{T}}}\right)\left(2-\frac{1}{N_{\text{R}}}\right) - \sigma_{\text{g}}^4 \approx 3\sigma_{\text{g}}^4$ and approximation holds true when antenna array size N_{R} and N_{T} are large. Therefore, according to CLT $\gamma_{\text{PT},1}$ is Gaussian distributed with mean and variance $\mathbb{E}(\gamma_{\text{PT},1}) = \sigma_{\text{g}}^2 + \mu_{\text{PT},0}$ and $\text{var}(\gamma_{\text{PT},1}) = 3\sigma_{\text{g}}^4/M + \sigma_{\text{PT},0}^2$. The miss detection probability $P_{\text{MD,PT}} = \text{Q}[(\mathbb{E}(\gamma_{\text{PT},1}) - \eta_{\text{PT}})/\sqrt{\text{var}(\gamma_{\text{PT},1})}]$ reduces to (10) after plug-in the expression of $\mathbb{E}(\gamma_{\text{PT},1})$ and $\text{var}(\gamma_{\text{PT},1})$, expression of $\eta_{\text{PT}}^\star$ in (8), and definition of SNR.

With no synchronization, the detection statistic under $\mathcal{H}_1$ is denoted as $\gamma_{\text{NT},1}$. The exact distribution of $\gamma_{\text{NT},1}$ is challenging. We make the following approximation to simplify the derivation: 1) the energy of $\gamma_{\text{NT},1}$ corresponding to the true correlation peaks plus noise power; 2) the non-aligned beamformer due to abrupt beamformer change results in independent $\mathbf{v}_m$ and $\mathbf{w}_m$. Based on

this assumption, we evaluate distribution of $\gamma_{\mathrm{NT},1}$ by considering the impact of TO and CFO in the following $\gamma_{\mathrm{NT},1} = \frac{1}{MLN_{\mathrm{T}}N_{\mathrm{R}}}\sum_{m=1}^{M}\sum_{l=0}^{L}|\tilde{g}_{m,l}^{(1)}\sum_{n_1=1}^{K-1}|s[n_1]|^2 e^{j\epsilon_{\mathrm{F}}n_1} + \tilde{g}_{m,l}^{(2)}\sum_{n_2=K}^{P}|s[n_2]|^2 e^{j\epsilon_{\mathrm{F}}n_2}|^2 + \gamma_{\mathrm{PT},0}$ where $\tilde{g}_{m,l}^{(1)} = g_l\mathbf{w}_m^{\mathrm{H}}\mathbf{a}_{\mathrm{R}}(\phi_l)\mathbf{a}_{\mathrm{T}}^{\mathrm{H}}(\theta_l)\mathbf{v}_m$ and $\tilde{g}_{m,l}^{(2)} = g_l\mathbf{w}_{m+1}^{\mathrm{H}}\mathbf{a}_{\mathrm{R}}(\phi_l)\mathbf{a}_{\mathrm{T}}^{\mathrm{H}}(\theta_l)\mathbf{v}_m$ are the post-beamforming channel gain due to partially overlapped burst window in BS and UE. In other word, K follows (12) and $n_1 \in [1, K-1]$ and $n_2 \in [K, P]$ are the sample window with K represents the abrupt change in beamformer. Based on the assumption of independent $\mathbf{w}_m$ and $\mathbf{w}_{m+1}$, $\tilde{g}_{m,l}^{(1)}$ it is straightforward to show that $\tilde{g}_{m,l}^{(2)}$ are uncorrelated. For notational convenience of finding statistic of $\gamma_{\mathrm{NT},1}$, we define $\zeta_{m,l}$ as $\zeta_{m,l} \triangleq (|\tilde{g}_{m,l}^{(1)}\frac{1-e^{jK\epsilon_{\mathrm{F}}}}{1-e^{j\epsilon_{\mathrm{F}}}} + \tilde{g}_{m,l}^{(2)}\frac{1-e^{j(P-K)\epsilon_{\mathrm{F}}}}{1-e^{j\epsilon_{\mathrm{F}}}}|^2)/(N_{\mathrm{T}}N_{\mathrm{R}}P^2)$ in $\gamma_{\mathrm{NT},1}$ after simplification with the fact $|s[n]|^2 = 1/P, \forall n \in \mathcal{S}$ as well as $\sum_{n=1}^{K} e^{j\epsilon_{\mathrm{T}}n} = (1-e^{jK\epsilon_{\mathrm{F}}})/(1-e^{j\epsilon_{\mathrm{F}}})$. The mean of $\zeta_{m,l}$ is $\mathbb{E}(\zeta_{m,l}) = \kappa(\epsilon_{\mathrm{F}},\epsilon_{\mathrm{T}})\sigma_{\mathrm{g}}^2$ after plug-in definition in (11). The variance of $\zeta_{m,l}$ is $\mathrm{var}(\zeta_{m,l}) \approx 2\sigma_{\mathrm{g}}^4\zeta^2(\epsilon_{\mathrm{F}},\epsilon_{\mathrm{T}})$. This is a straightforward extension of derivation and approximation in Appendix A. Using CLT and statistic of $\zeta_{m,l}$, we conclude that $\gamma_{\mathrm{NT},1}$ is Gaussian distributed with mean and variance to be $\mathbb{E}(\gamma_{\mathrm{NT},1}) = \kappa(\epsilon_{\mathrm{F}},\epsilon_{\mathrm{T}})\sigma_{\mathrm{g}}^2 + \mu_{\mathrm{PT},0}$ and $\mathrm{var}(\gamma_{\mathrm{NT},1}) = 2\sigma_{\mathrm{g}}^4\kappa^2(\epsilon_{\mathrm{F}},\epsilon_{\mathrm{T}})/M + \sigma_{\mathrm{PT},0}^2$, respectively. The miss detection probability $P_{\mathrm{MD,NT}} = \mathrm{Q}[(\mathbb{E}(\gamma_{\mathrm{NT},1}) - \eta_{\mathrm{NT}}^{\star})/\sqrt{\mathrm{var}(\gamma_{\mathrm{NT},1})}]$ reduces to (10) once one plug-in expressions of $\mu_{\mathrm{NT},0}$, $\eta_{\mathrm{NT}}^{\star}$, and $\gamma_{\mathrm{NT},1}$ and definition of SNR.

B. CRLB of joint estimation problem

The FIM has the following form

$$\mathbf{J} = \frac{1}{\sigma_{\mathrm{n}}^2}\begin{bmatrix} \Phi_{\epsilon_{\mathrm{F}},\epsilon_{\mathrm{F}}} & \Phi_{\epsilon_{\mathrm{F}},\theta} & \Phi_{\epsilon_{\mathrm{F}},\phi} & \Phi_{\epsilon_{\mathrm{F}},\tau} & \Phi_{\epsilon_{\mathrm{F}},\alpha} & \Phi_{\epsilon_{\mathrm{F}},\beta} \\ \Phi_{\theta,\epsilon_{\mathrm{F}}} & \Phi_{\theta,\theta} & \Phi_{\theta,\phi} & \Phi_{\theta,\tau} & \Phi_{\theta,\alpha} & \Phi_{\theta,\beta} \\ \Phi_{\phi,\epsilon_{\mathrm{F}}} & \Phi_{\phi,\theta} & \Phi_{\phi,\phi} & \Phi_{\phi,\tau} & \Phi_{\phi,\alpha} & \Phi_{\phi,\beta} \\ \Phi_{\tau,\epsilon_{\mathrm{F}}} & \Phi_{\tau,\theta} & \Phi_{\tau,\phi} & \Phi_{\tau,\tau} & \Phi_{\tau,\alpha} & \Phi_{\tau,\beta} \\ \Phi_{\alpha,\epsilon_{\mathrm{F}}} & \Phi_{\alpha,\theta} & \Phi_{\alpha,\phi} & \Phi_{\alpha,\tau} & \Phi_{\alpha,\alpha} & 0 \\ \Phi_{\beta,\epsilon_{\mathrm{F}}} & \Phi_{\beta,\theta} & \Phi_{\beta,\phi} & \Phi_{\beta,\tau} & 0 & \Phi_{\beta,\beta} \end{bmatrix} \tag{34}$$

where $\Phi_{x,x}$ denotes for $\Phi_{x,x} = \partial^2 L(\mathbf{y};\boldsymbol{\xi})/\partial x\partial y = (\partial L(\mathbf{x}(\boldsymbol{\xi})/\partial x)^{\mathrm{H}}(\partial L(\mathbf{x}(\boldsymbol{\xi}))/\partial y)$.

The exact expression of each elements in FIM are summarized in Table IV, where or notational convenience the following matrices are defined. The derivative over CFO matrix is a diagonal matrix whose p-th diagonal element is $\{\dot{\mathbf{Q}}_m\}_p = j[(m-1)N_{\mathrm{B}} + (p-1)]e^{j\epsilon_{\mathrm{F}}[(m-1)N_{\mathrm{B}}+(p-1)]}$. The vector $\mathbf{f}(\tau)$ is the frequency support due to delay τ as $\mathbf{f}(\tau) = [1, e^{j\frac{2\pi T_{\mathrm{s}}}{\tau}}, \cdots, e^{j\frac{2\pi PT_{\mathrm{s}}}{\tau}}]^{\mathrm{T}}$, and its derivative $\dot{\mathbf{f}} = \partial\mathbf{f}(\tau)/\partial\tau$ whose p-th element is $\{\dot{\mathbf{f}}\}_p = j2\pi(p-1)T_{\mathrm{s}}e^{j2\pi(p-1)\epsilon_{\mathrm{F}}T_{\mathrm{s}}}$

Further, note that the following simplification is used. $\mathbf{f}^{\mathrm{H}}(\tau)\mathbf{F}^{\mathrm{H}}\mathbf{Q}_m^{\mathrm{H}}\mathbf{Q}_m\mathbf{F}\mathbf{f}(\tau) = P, \forall m$ and define scaler constant $C_{\mathrm{df}} = \sum_{p=0}^{P-1} 2\pi pT_{\mathrm{s}} = (P-2)(P-1)\pi T_{\mathrm{s}}$ and define scaler constant $C_{\mathrm{dq},m} \triangleq \mathbf{f}^{\mathrm{H}}(\tau)\mathbf{F}^{\mathrm{H}}\dot{\mathbf{Q}}_m^{\mathrm{H}}\mathbf{Q}_m\mathbf{F}\mathbf{f}(\tau) = (m-1)T_{\mathrm{B}} + \frac{(P-2)(P-1)T_{\mathrm{s}}}{2}$, and define scaler constant $C_{\mathrm{d2q},m} \triangleq \mathbf{f}^{\mathrm{H}}(\tau)\dot{\mathbf{Q}}_m^{\mathrm{H}}\dot{\mathbf{Q}}_m\mathbf{f}(\tau) = \sum_{p=0}^{P-1}[(m-1)T_{\mathrm{B}} + pT_{\mathrm{s}}]^2$.

REFERENCES

[1] H. Yan and D. Cabric, "Compressive sensing based initial beamforming training for massive MIMO millimeter-wave systems," in *2016 IEEE Global Conference on Signal and Information Processing (GlobalSIP)*, Dec. 2016, pp. 620–624.

[2] J. G. Andrews, S. Buzzi, W. Choi, S. V. Hanly, A. Lozano, A. C. K. Soong, and J. C. Zhang, "What will 5G be?" *IEEE J. Sel. Areas Commun.*, vol. 32, no. 6, pp. 1065–1082, Jun. 2014.

[3] T. S. Rappaport, S. Sun, R. Mayzus, H. Zhao, Y. Azar, K. Wang, G. N. Wong, J. K. Schulz, M. Samimi, and F. Gutierrez, "Millimeter wave mobile communications for 5G cellular: It will work!" *IEEE Access*, vol. 1, pp. 335–349, May 2013.

[4] R. W. Heath, N. Gonzlez-Prelcic, S. Rangan, W. Roh, and A. M. Sayeed, "An overview of signal processing techniques for millimeter wave MIMO systems," *IEEE J. Sel. Topics Signal Process.*, vol. 10, no. 3, pp. 436–453, Apr. 2016.

[5] 3GPP, "TR38.802 study on new radio access technology physical layer aspects," 2017. [Online]. Available: https://portal.3gpp.org/desktopmodules/Specifications

[6] C. N. Barati, S. A. Hosseini, S. Rangan, P. Liu, T. Korakis, S. S. Panwar, and T. S. Rappaport, "Directional cell discovery in millimeter wave cellular networks," *IEEE Trans. Wireless Commun.*, vol. 14, no. 12, pp. 6664–6678, Dec. 2015.

[7] M. Giordani, M. Polese, A. Roy, D. Castor, and M. Zorzi, "A tutorial on beam management for 3GPP NR at mmWave frequencies," *CoRR*, vol. abs/1804.01908, 2018. [Online]. Available: http://arxiv.org/abs/1804.01908

[8] Y. Li, J. Luo, M. H. C. Garcia, R. Bhnke, R. A. Stirling-Gallacher, W. Xu, and G. Caire, "On the beamformed broadcasting for millimeter wave cell discovery: Performance analysis and design insight," vol. 17, no. 11, pp. 7620–7634, Nov. 2018.

[9] Y. Li, F. Baccelli, J. G. Andrews, and J. C. Zhang, "Directional cell search delay analysis for cellular networks with static users," *IEEE Trans. Commun.*, pp. 1–1, 2018.

[10] Y. Yang, H. S. Ghadikolaei, C. Fischione, M. Petrova, and K. W. Sung, "Reducing initial cell-search latency in mmWave networks," *CoRR*, vol. abs/1802.06450, 2018. [Online]. Available: http://arxiv.org/abs/1802.06450

[11] X. Meng, X. Gao, and X. G. Xia, "Omnidirectional precoding and combining based synchronization for millimeter wave massive MIMO systems," *IEEE Transactions on Communications*, vol. 66, no. 3, pp. 1013–1026, Mar. 2018.

[12] M. Giordani, M. Mezzavilla, and M. Zorzi, "Initial access in 5G mmWave cellular networks," *IEEE Commun. Mag.*, vol. 54, no. 11, pp. 40–47, Nov. 2016.

[13] A. Alkhateeb, Y. H. Nam, M. S. Rahman, J. Zhang, and R. W. Heath, "Initial beam association in millimeter wave cellular systems: Analysis and design insights," *IEEE Trans. Wireless Commun.*, vol. 16, no. 5, pp. 2807–2821, May 2017.

[14] A. Alkhateeb, O. E. Ayach, G. Leus, and R. W. Heath, "Channel estimation and hybrid precoding for millimeter wave cellular systems," *IEEE J. Sel. Topics Signal Process.*, vol. 8, no. 5, pp. 831–846, Oct. 2014.

[15] C. Liu, M. Li, S. V. Hanly, I. B. Collings, and P. Whiting, "Millimeter wave beam alignment: Large deviations analysis and design insights," *IEEE J. Sel. Areas Commun.*, vol. 35, no. 7, pp. 1619–1631, Jul. 2017.

[16] Z. Marzi, D. Ramasamy, and U. Madhow, "Compressive channel estimation and tracking for large arrays in mm wave picocells," *IEEE J. Sel. Topics Signal Process.*, vol. PP, no. 99, pp. 1–1, Apr. 2016.

[17] A. Alkhateeby, G. Leusz, and R. W. Heath, "Compressed sensing based multi-user millimeter wave systems: How many measurements are needed?" in *2015 IEEE International Conference on Acoustics, Speech and Signal Processing (ICASSP)*, Apr. 2015, pp. 2909–2913.

[18] J. Rodrguez-Fernndez, N. Gonzlez-Prelcic, K. Venugopal, and R. W. Heath, "Frequency-domain compressive channel estimation for frequency-selective hybrid millimeter wave MIMO systems," *IEEE Trans. Wireless Commun.*, vol. 17, no. 5, pp. 2946–2960, May 2018.

[19] Y. Wang, Z. Tian, S. Feng, and P. Zhang, "Efficient channel statistics estimation for millimeter-wave MIMO systems," in *2016 IEEE International Conference on Acoustics, Speech and Signal Processing (ICASSP)*, Mar. 2016, pp. 3411–3415.

[20] X. Song, S. Haghighatshoar, and G. Caire, "A scalable and statistically robust beam alignment technique for millimeter-wave systems," *IEEE Trans. Wireless Commun.*, vol. 17, no. 7, pp. 4792–4805, Jul. 2018.

TABLE IV
ELEMENTS OF FISHER INFORMATION MATRIX

Symb.	Expressions	Symb.	Expressions
$\Phi_{\epsilon_{\mathrm{F}},\epsilon_{\mathrm{F}}}$	$\sum_{m=1}^{M}(C_{\mathrm{d2q}}g)\left\|\mathbf{w}_m^{\mathrm{H}}\mathbf{a}_{\mathrm{R}}(\phi)\right\|^2\left\|\mathbf{v}_m^{\mathrm{H}}\mathbf{a}_{\mathrm{T}}(\theta)\right\|^2$	$\Phi_{\epsilon_{\mathrm{F}},\theta}$	$\sum_{m=1}^{M}(C_m g)\left\|\mathbf{w}_m^{\mathrm{H}}\mathbf{a}_{\mathrm{R}}(\phi)\right\|^2\Re\left\{\left[\mathbf{v}_m^{\mathrm{H}}\dot{\mathbf{a}_{\mathrm{T}}}(\theta)\right]\left[\mathbf{v}_m^{\mathrm{H}}\mathbf{a}_{\mathrm{T}}(\theta)\right]\right\}$
$\Phi_{\epsilon_{\mathrm{F}},\tau}$	$\Re\left\{\sum_{m=1}^{M}g\left\|\mathbf{w}_m^{\mathrm{H}}\mathbf{a}_{\mathrm{R}}(\phi)\right\|^2\left\|\mathbf{v}_m^{\mathrm{H}}\mathbf{a}_{\mathrm{T}}(\theta)\right\|^2\mathbf{f}^{\mathrm{H}}(\tau)\mathbf{F}\dot{\mathbf{Q}}_m^{\mathrm{H}}\mathbf{Q}_m\mathbf{F}^{\mathrm{H}}\hat{\mathbf{f}}(\tau)\right\}$	$\Phi_{\epsilon_{\mathrm{F}},\alpha}$	$\sum_{m=1}^{M}\left[C_{\mathrm{dq},m}\Re(g)\right]\left\|\mathbf{w}_m^{\mathrm{H}}\mathbf{a}_{\mathrm{R}}(\phi)\right\|^2\left\|\mathbf{v}_m^{\mathrm{H}}\mathbf{a}_{\mathrm{T}}(\theta)\right\|^2$
$\Phi_{\epsilon_{\mathrm{F}},\beta}$	$\sum_{m=1}^{M}\left[C_{\mathrm{dq},m}\Im(g)\right]\left\|\mathbf{w}_m^{\mathrm{H}}\mathbf{a}_{\mathrm{R}}(\phi)\right\|^2\left\|\mathbf{v}_m^{\mathrm{H}}\mathbf{a}_{\mathrm{T}}(\theta)\right\|^2$	$\Phi_{\theta,\theta}$	$\sum_{m=1}^{M}(P\lvert g\rvert^2)\left\|\mathbf{w}_m^{\mathrm{H}}\mathbf{a}_{\mathrm{R}}(\phi)\right\|^2\left\|\mathbf{v}_m^{\mathrm{H}}\dot{\mathbf{a}_{\mathrm{T}}}(\theta)\right\|^2$
$\Phi_{\phi,\phi}$	$\sum_{m=1}^{M}(P\lvert g\rvert^2)\left\|\mathbf{w}_m^{\mathrm{H}}\dot{\mathbf{a}}_{\mathrm{R}}(\phi)\right\|^2\left\|\mathbf{v}_m^{\mathrm{H}}\mathbf{a}_{\mathrm{T}}(\theta)\right\|^2$	$\Phi_{\phi,\theta}$	$\Re\left\{\sum_{m=1}^{M}P\lvert g\rvert^2[\mathbf{w}_m^{\mathrm{H}}\mathbf{a}_{\mathrm{R}}(\phi)][\mathbf{w}_m^{\mathrm{H}}\dot{\mathbf{a}}_{\mathrm{R}}(\phi)][\mathbf{v}_m^{\mathrm{H}}\dot{\mathbf{a}}_{\mathrm{T}}(\theta)][\mathbf{v}_m^{\mathrm{H}}\mathbf{a}_{\mathrm{T}}(\theta)]\right\}$
$\Phi_{\phi,\tau}$	$\sum_{m=1}^{M}C_{\mathrm{df},m}\lvert g\rvert^2\Re\left\{[\mathbf{w}_m^{\mathrm{H}}\dot{\mathbf{a}}_{\mathrm{R}}(\phi)][\mathbf{w}_m^{\mathrm{H}}\mathbf{a}_{\mathrm{R}}(\phi)]\right\}\left\|\mathbf{v}_m^{\mathrm{H}}\mathbf{a}_{\mathrm{T}}(\theta)\right\|^2$	$\Phi_{\phi,\alpha}$	$\Re\left\{\sum_{m=1}^{M}Pg[\mathbf{w}_m^{\mathrm{H}}\dot{\mathbf{a}}_{\mathrm{R}}(\phi)][\mathbf{w}_m^{\mathrm{H}}\mathbf{a}_{\mathrm{R}}(\phi)]\lvert\mathbf{v}_m^{\mathrm{H}}\mathbf{a}_{\mathrm{T}}(\theta)\rvert^2\right\}$
$\Phi_{\theta,\alpha}$	$\Re\left\{\sum_{m=1}^{M}Pg\lvert\mathbf{w}_m^{\mathrm{H}}\mathbf{a}_{\mathrm{R}}(\phi)\rvert^2[\mathbf{v}_m^{\mathrm{H}}\dot{\mathbf{a}}_{\mathrm{T}}(\theta)][\mathbf{v}_m^{\mathrm{H}}\mathbf{a}_{\mathrm{T}}(\theta)]\right\}$	$\Phi_{\phi,\beta}$	$\Re\left\{\sum_{m=1}^{M}jgP[\mathbf{w}_m^{\mathrm{H}}\dot{\mathbf{a}}_{\mathrm{R}}(\phi)][\mathbf{w}_m^{\mathrm{H}}\mathbf{a}_{\mathrm{R}}(\phi)]\lvert\mathbf{v}_m^{\mathrm{H}}\mathbf{a}_{\mathrm{T}}(\theta)\rvert^2\right\}$
$\Phi_{\theta,\beta}$	$\Re\left\{\sum_{m=1}^{M}jPg\lvert\mathbf{w}_m^{\mathrm{H}}\mathbf{a}_{\mathrm{R}}(\phi)\rvert^2[\mathbf{v}_m^{\mathrm{H}}\dot{\mathbf{a}}_{\mathrm{T}}(\theta)][\mathbf{v}_m^{\mathrm{H}}\mathbf{a}_{\mathrm{T}}(\theta)]\right\}$	$\Phi_{\tau,\tau}$	$\Re\left\{\sum_{m=1}^{M}\lvert g\rvert^2\lvert\mathbf{w}_m^{\mathrm{H}}\mathbf{a}_{\mathrm{R}}(\phi)\rvert^2\lvert\mathbf{v}_m^{\mathrm{H}}\mathbf{a}_{\mathrm{T}}(\theta)\rvert^2\left[\dot{\mathbf{f}}^{\mathrm{H}}(\tau)\mathbf{Q}_m^{\mathrm{H}}\mathbf{Q}_m\dot{\mathbf{f}}(\tau)\right]\right\}$
$\Phi_{\tau,\alpha}$	$\Re\left\{\sum_{m=1}^{M}g\lvert\mathbf{w}_m^{\mathrm{H}}\mathbf{a}_{\mathrm{R}}(\phi)\rvert^2\lvert\mathbf{v}_m^{\mathrm{H}}\mathbf{a}_{\mathrm{T}}(\theta)\rvert^2\left[\dot{\mathbf{f}}^{\mathrm{H}}(\tau)\mathbf{Q}_m^{\mathrm{H}}\mathbf{Q}_m\mathbf{f}(\tau)\right]\right\}$	$\Phi_{\tau,\beta}$	$\Re\left\{\sum_{m=1}^{M}jg\lvert\mathbf{w}_m^{\mathrm{H}}\mathbf{a}_{\mathrm{R}}(\phi)\rvert^2\lvert\mathbf{v}_m^{\mathrm{H}}\mathbf{a}_{\mathrm{T}}(\theta)\rvert^2\left[\dot{\mathbf{f}}^{\mathrm{H}}(\tau)\mathbf{Q}_m^{\mathrm{H}}\mathbf{Q}_m\mathbf{f}(\tau)\right]\right\}$
$\Phi_{\alpha,\alpha}$	$\sum_{m=1}^{M}P\lvert\mathbf{w}_m^{\mathrm{H}}\mathbf{a}_{\mathrm{R}}(\phi)\rvert^2\lvert\mathbf{v}_m^{\mathrm{H}}\mathbf{a}_{\mathrm{T}}(\theta)\rvert^2$	$\Phi_{\beta,\beta}$	$-\sum_{m=1}^{M}P\lvert\mathbf{w}_m^{\mathrm{H}}\mathbf{a}_{\mathrm{R}}(\phi)\rvert^2\lvert\mathbf{v}_m^{\mathrm{H}}\mathbf{a}_{\mathrm{T}}(\theta)\rvert^2$

[21] S. Park and R. W. Heath, "Spatial channel covariance estimation for the hybrid MIMO architecture: A compressive sensing-based approach," *IEEE Trans. Wireless Commun.*, vol. 17, no. 12, pp. 8047–8062, Dec. 2018.

[22] J. P. Gonzlez-Coma, J. Rodrguez-Fernndez, N. Gonzlez-Prelcic, L. Castedo, and R. W. Heath, "Channel estimation and hybrid precoding for frequency selective multiuser mmwave MIMO systems," *IEEE J. Sel. Topics Signal Process.*, vol. 12, no. 2, pp. 353–367, May 2018.

[23] L. Zhao, D. W. K. Ng, and J. Yuan, "Multi-user precoding and channel estimation for hybrid millimeter wave systems," *IEEE J. Sel. Areas Commun.*, vol. 35, no. 7, pp. 1576–1590, Jul. 2017.

[24] N. J. Myers and R. W. Heath, "A compressive channel estimation technique robust to synchronization impairments," in *2017 IEEE 18th International Workshop on Signal Processing Advances in Wireless Communications (SPAWC)*, Jul. 2017, pp. 1–5.

[25] M. Pajovic, P. Wang, T. Koike-Akino, and P. Orlik, "Estimation of frequency unsynchronized millimeter-wave channels," in *2017 IEEE Global Conference on Signal and Information Processing (GlobalSIP)*, Nov. 2017, pp. 1205–1209.

[26] N. J. Myers and R. W. Heath, "Message passing-based joint CFO and channel estimation in millimeter wave systems with one-bit adcs," *CoRR*, vol. abs/1803.09012, 2018. [Online]. Available: http://arxiv.org/abs/1803.09012

[27] M. E. Rasekh, Z. Marzi, Y. Zhu, U. Madhow, and H. Zheng, "Noncoherent mmWave path tracking," in *Proceedings of the 18th International Workshop on Mobile Computing Systems and Applications*, ser. HotMobile '17. New York, NY, USA: ACM, 2017, pp. 13–18. [Online]. Available: http://doi.acm.org/10.1145/3032970.3032974

[28] H. Hassanieh, O. Abari, M. Rodriguez, M. Abdelghany, D. Katabi, and P. Indyk, "Fast millimeter wave beam alignment," in *Proceedings of the 2018 Conference of the ACM Special Interest Group on Data Communication*, ser. SIGCOMM '18. New York, NY, USA: ACM, 2018, pp. 432–445. [Online]. Available: http://doi.acm.org/10.1145/3230543.3230581

[29] M. E. Rasekh and U. Madhow, "Noncoherent compressive channel estimation for mm-wave massive MIMO," *CoRR*, vol. abs/1801.06608, 2018. [Online]. Available: http://arxiv.org/abs/1801.06608

[30] C. Li and W. Huang, "A constructive representation for the Fourier dual of the Zadoff-Chu sequences," vol. 53, no. 11, pp. 4221–4224, Nov. 2007.

[31] 3GPP, "TS38.211 NR physical channels and modulation (release 15)," 2018. [Online]. Available: https://portal.3gpp.org

[32] J. Song, J. Choi, and D. J. Love, "Common codebook millimeter wave beam design: Designing beams for both sounding and communication with uniform planar arrays," *IEEE Trans. Commun.*, vol. 65, no. 4, pp. 1859–1872, Apr. 2017.

[33] T. S. Rappaport, G. R. MacCartney, M. K. Samimi, and S. Sun, "Wideband millimeter-wave propagation measurements and channel models for future wireless communication system design," *IEEE Trans. Commun.*, vol. 63, no. 9, pp. 3029–3056, Sep. 2015.

[34] 5GPPP, "D2.2 measurement results and final mmMAGIC channel models," *Tech. Rep.* [Online]. Available: https://5g-mmmagic.eu/results

[35] S. J. Orfinidas, *Electromagnetic Waves and Antennas*, Feb. 2017. [Online]. Available: http://www.ece.rutgers.edu/orfanidi/ewa/

[36] S. Kay, "A fast and accurate single frequency estimator," *IEEE Transactions on Acoustics, Speech, and Signal Processing*, vol. 37, no. 12, pp. 1987–1990, Dec. 1989.

[37] D. Malioutov, M. Cetin, and A. S. Willsky, "A sparse signal reconstruction perspective for source localization with sensor arrays," *IEEE Trans. Signal Process.*, vol. 53, no. 8, pp. 3010–3022, Aug. 2005.

[38] L. Jacques and C. D. Vleeschouwer, "A geometrical study of matching pursuit parametrization," *IEEE Trans. Signal Process.*, vol. 56, no. 7, pp. 2835–2848, Jul. 2008.

[39] B. Mamandipoor, D. Ramasamy, and U. Madhow, "Newtonized orthogonal matching pursuit: Frequency estimation over the continuum," *IEEE Trans. Signal Process.*, vol. 64, no. 19, pp. 5066–5081, Oct. 2016.

[40] M. R. Castellanos, V. Raghavan, J. H. Ryu, O. H. Koymen, J. Li, D. J. Love, and B. Peleato, "Channel-reconstruction-based hybrid precoding for millimeter-wave multi-user MIMO systems," *IEEE J. Sel. Topics Signal Process.*, vol. 12, no. 2, pp. 383–398, May 2018.

[41] U. Kodak and G. M. Rebeiz, "Bi-directional flip-chip 28 GHz phased-array core-chip in 45nm CMOS SOI for high-efficiency high-linearity 5G systems," in *2017 IEEE Radio Frequency Integrated Circuits Symposium (RFIC)*, Jun. 2017, pp. 61–64.

[42] D. D. Donno, J. Palacios, and J. Widmer, "Millimeter-wave beam training acceleration through low-complexity hybrid transceivers," *IEEE Trans. Wireless Commun.*, vol. 16, no. 6, pp. 3646–3660, Jun. 2017.

[43] S. Jaeckel, L. Raschkowski, K. Brner, and L. Thiele, "QuaDRiGa: A 3-D multi-cell channel model with time evolution for enabling virtual field trials," *IEEE Trans. Antennas Propag.*, vol. 62, no. 6, pp. 3242–3256, Jun. 2014.

[44] A. Demir, A. Mehrotra, and J. Roychowdhury, "Phase noise in oscillators: a unifying theory and numerical methods for characterization," *IEEE Trans. Circuits Syst. I*, vol. 47, no. 5, pp. 655–674, May 2000.

[45] Y. Qi, M. Hunukumbure, H. Nam, H. Yoo, and S. Amuru, "On the phase tracking reference signal (PT-RS) design for 5G new radio (NR)," *CoRR*, vol. abs/1807.07336, 2018. [Online]. Available: http://arxiv.org/abs/1807.07336

[46] W. El-Halwagy, A. Nag, P. Hisayasu, F. Aryanfar, P. Mousavi, and M. Hossain, "A 28GHz quadrature fractional-N synthesizer for 5G mobile communication with less than 100fs jitter in 65nm CMOS," in *2016 IEEE Radio Frequency Integrated Circuits Symposium (RFIC)*, May 2016, pp. 118–121.

[47] H. Yan, "Matlab simulation for millimeter-wave compressive initial access and beam training," 2019. [Online]. Available: https://github.com/yhaddint/MillimeterWaveCSIA

[48] 3GPP, "Finalization of the NR-SSS," *Huawei, HiSilicon - Tdoc R1-1709901*, Jun. 2017.

[49] ——, "TR38.901 study on channel model for frequencies from 0.5 to 100 GHz," *Tech. Rep.*, 2017. [Online]. Available: https://portal.3gpp.org

[50] A. Alkhateeb, G. Leus, and R. W. Heath, "Limited feedback hybrid precoding for multi-user millimeter wave systems," *IEEE Trans. Wireless Commun.*, vol. 14, no. 11, pp. 6481–6494, Nov. 2015.

[51] D. E. Berraki, T. H. Barratt, M. A. Beach, S. M. D. Armour, and A. R. Nix, "Practical demonstration of limited feedback beamforming for

mmWave systems," in *2015 IEEE 81st Vehicular Technology Conference (VTC Spring)*, May 2015, pp. 1–5.

[52] X. Yang, M. Matthaiou, J. Yang, C. Wen, F. Gao, and S. Jin, "Hardware-constrained millimeter wave systems for 5G: Challenges, opportunities, and solutions," *CoRR*, vol. abs/1811.03269, 2018. [Online]. Available: http://arxiv.org/abs/1811.03269